

This is to certify that the thesis entitled

A SIMPLE AND ACCURATE METHOD FOR THE SHOCK MODE CALIBRATION OF PIEZOELECTRIC ACCELEROMETERS

presented by

Thomas Jeremy Bruno

has been accepted towards fulfillment of the requirements for the

Master of Science degree in School of Packaging

Major Professor's Signature

1-91-0

Date

MSU is an Affirmative Action/Equal Opportunity Institution

LIBRARY
Michic State
University

PLACE IN RETURN BOX to remove this checkout from your record. TO AVOID FINES return on or before date due. MAY BE RECALLED with earlier due date if requested.

DATE DUE	DATE DUE	DATE DUE
		,
		,
	-	

2/05 p:/CIRC/DateDue.indd-p.1

A SIMPLE AND ACCURATE METHOD FOR THE SHOCK MODE CALIBRATION OF PIEZOELECTRIC ACCELEROMETERS

Ву

Thomas Jeremy Bruno

A THESIS

Submitted to
Michigan State University
in partial fulfillment of the requirements
for the degree of

MASTER OF SCIENCE

School of Packaging

2006

ABSTRACT

A SIMPLE AND ACCURATE METHOD FOR THE SHOCK MODE CALIBRATION OF PIEZOELECTRIC ACCELEROMETERS

By

Thomas Jeremy Bruno

Absolute methods of accelerometer calibration while being subjected to shock are generally unavailable, and the need for a method of calibration that simulates an actual use situation, such as shock, has long been overlooked.

The proposed method is an absolute method of calibration that can be used to determine, within 5%, the sensitivity of a piezoelectric accelerometer while being subjected to shock. It is also insensitive to filtering and acceptable for use throughout a range of g levels common to the packaging industry.

The method involves an accelerometer mounted onto the head of a hammer. The hammer, including accelerometer, is released to rotate onto any suitable impact surface. Video recording captures the drop, and the rebound angle of the hammer is measured through the slow motion replay of the video.

The method is designed to be an in-house supplement to packaging laboratory equipment that is inexpensive to manufacture and cost effective to implement. It provides a quick and accurate method to generate confidence in the sensitivity of piezoelectric accelerometers at any point throughout their lifespan without the use of reference or special equipment.

ACKNOWLEDGMENTS

I would like to express my appreciation to my major advisor, Dr. Gary
Burgess, for the guidance, advice, and support he provided towards the
completion of this thesis. I would also like to thank my committee members Dr.
Paul Singh and Dr. Brian Feeny for their valuable comments.

TABLE OF CONTENTS

LIST OF TABLES	vii
LIST OF FIGURES	ix
KEY TO SYMBOLS	xi
CHAPTER 1	
PEIZOELECTRIC ACCELEROMETERS	
Description	
Performance Characteristics	4
System Setup	
Mounting Techniques	
Shock Pulse Information	
Filtering	
Calibration Techniques	
Cost	17
Objectives	18
Concept	20
CHAPTER 2	
MATERIALS AND METHODS	22
Description of Calibration Device	
Method of Use	
Natural Frequency	
Change in Velocity	
Theory	
Simple Harmonic Motion of a Pendulum	
Sensitivity	
Set isitivity	
CHAPTER 3	
RESULTS	39
Natural Frequency	
Rebound Angles	
Correction Factor	
Impact Surfaces	
Signal Filtering	
ΔV_{actual} vs ΔV_{pulse}	53
Remounting Results	

TABLE OF CONTENTS (con't)

CHAPTER 4	
CONCLUSIONS	59
Method Accuracy	59
Recommendations of Use	
Design Recommendations	63
APPENDICES	64
BIBLIOGRAPHY	92
GENERAL RESOURCES	94

LIST OF TABLES

TABLE 1:	Natural Frequency Results40
TABLE A-1:	Manual Filter Frequency for Rubber Impact Surface67
TABLE A-2:	Manual Filter Frequency for Compressed Air Impact Surface68
TABLE A-3:	Manual Filter Frequency for 2 pcf Foam Cushion Impact Surface
TABLE B-1:	Results – Rubber Impact Surface and Auto Filter72
TABLE B-2:	Results – Rubber Impact Surface and No Filter73
TABLE B-3:	Results – Rubber Impact Surface and Manual Filter74
TABLE B-4:	Results – Compressed Air Impact Surface and Auto Filter75
TABLE B-5:	Results – Compressed Air Impact Surface and No Filter76
TABLE B-6:	Results – Compressed Air Impact Surface and Manual Filter77
TABLE B-7:	Results – 2 pcf Foam Impact Surface and Auto Filter78
TABLE B-8:	Results – 2 pcf Foam Impact Surface and No Filter79
TABLE B-9:	Results – 2 pcf Foam Impact Surface and Manual Filter80
TABLE C-1:	Remount Results - Rubber Impact Surface and Auto Filter83
TABLE C-2:	Remount Results – Rubber Impact Surface and No Filter84
TABLE C-3:	Remount Results – Rubber Impact Surface and Manual Filter85
TABLE C-4:	Remount Results – Compressed Air Impact Surface and Auto Filter
TABLE C-5:	Remount Results – Compressed Air Impact Surface and No Filter
TABLE C-6:	Remount Results – Compressed Air Impact Surface and Manual Filter

LIST OF TABLES (con't)

TABLE C-7:	Remount Results – 2 pcf Foam Impact Surface and Auto Filter	89
TABLE C-8:	Remount Results – 2 pcf Foam Impact Surface and No Filter	90
TABLE C-9:	Remount Results – 2 pcf Foam Impact Surface and Manual Filter	91

LIST OF FIGURES

FIGURE 1:	A Typical Piezoelectric Accelerometer	1
FIGURE 2:	Inside a Piezoelectric Accelerometer	2
FIGURE 3:	Typical Accelerometer System Setup	6
FIGURE 4:	Half-Sine Wave Shock Pulse	9
FIGURE 5:	Unfiltered Shock Pulse	.11
FIGURE 6:	Automatically Filtered Shock Pulse	.12
FIGURE 7:	Half-Sine Wave Shock Pulse – Area	.20
FIGURE 8:	Absolute Calibration Device – Shock	.23
FIGURE 9:	Absolute Calibration Device - Natural Frequency	.24
FIGURE 10:	Bearings	.25
FIGURE 11:	Absolute Shock Device – Angle of Impact	.26
FIGURE 12:	Absolute Shock Device – Release Angle	.30
FIGURE 13:	Variables Associated with the Theory	.32
FIGURE 14:	In Motion Rebound – Blurry Image	.41
FIGURE 15:	Maximum Rebound Angle – Sharp Image	.42
FIGURE 16:	Correction Factor – Automatic Filtering	.45
FIGURE 17:	Correction Factor – No Signal Filtering	.46
FIGURE 18:	Correction Factor – Manual Signal Filtering	.47
FIGURE 19:	Correction Factor – Rubber Impact Surface	.50
FIGURE 20:	Correction Factor – Compressed Air Impact Surface	.51
FIGURE 21:	Correction Factor – 2 pcf Foam Cushion Impact Surface	.52
FIGURE 22:	Δ _{actual} vs Δ _{pulse} – Rubber Impact Surface	.53

LIST OF FIGURES (con't)

FIGURE 23:	Δ_{actual} vs Δ_{pulse} – Compressed Air Impact Surface	54
FIGURE 24:	$\Delta_{ m actual}$ vs $\Delta_{ m pulse}$ – 2 pcf Foam Cushion Impact Surface	54
FIGURE 25:	Correction Factor After Remount – Rubber Impact Surface	56
FIGURE 26:	Correction Factor After Remount – Compressed Air Impact Surface	57
FIGURE 27:	Correction Factor After Remount – 2 pcf Foam Impact Surface	57

KEY TO SYMBOLS

A = amplitude of motion

a = distance from axle to the center of gravity of the hammer

 α = angular acceleration

b = distance from axle to the vertical axis of the accelerometer

 β = angle between tangent velocity and y-axis

f = correction factor

f_n = natural frequency

g = acceleration due to gravity

 h_d = drop height

h_r = rebound height

I_p = moment of inertia

KE = kinetic energy

m = mass

PE = potential energy

r = distance from the axle to the accelerometer

T = period

 τ = torque about a fixed axis of rotation

 θ_d = drop angle

 θ_r = rebound angle

∆V_{actual}= change in velocity measured from rebound height

 ΔV_{pulse} = change in velocity according to the shock pulse

KEY TO SYMBOLS (con"t)

- V_i = impact velocity
- V_r = rebound velocity
- V_y = vertical velocity
- ω = angular velocity

CHAPTER 1

PIEZOELECTRIC ACCELEROMETERS

1.1 DESCRIPTION

Accelerometers are devices used to measure acceleration. They are used by the auto industry to deploy airbags, the military to guide missiles, and, among others, the packaging industry to measure shock and vibration. There are many different types of accelerometers but most consist of the same basic principle; a seismic mass on a spring all housed in a stiff rugged casing. A typical accelerometer used in package testing applications is shown in Figure 1.

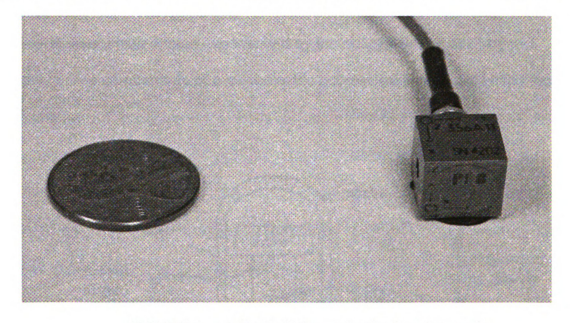


FIGURE 1: A Typical Piezoelectric Accelerometer

There are many categories of accelerometers that are classified by their sensing method, such as, capacitive, hall effect, heat transfer, piezoresistive, and piezoelectric.⁽¹⁾ Each of these categories uses either a different deflection sensing material or is designed for unique applications. Capacitive accelerometers measure the change in capacitance related to displacement. Hall

effect accelerometers sense changing magnetic fields during motion. Heat transfer accelerometers sense temperature changes during acceleration.

Piezoresistive accelerometers sense the change in electrical resistance during deflection, and piezoelectric accelerometers measure the piezoelectric effect of crystalline materials under an applied force. (1,7)

The deflection sensing materials used in piezoelectric accelerometers are crystalline materials, such as quartz or ceramic, and are used for their piezoelectric properties, meaning that, pressure induces strain which generates an electric signal.⁽⁷⁾ The electric signal generated by the seismic mass compressing the crystalline material is directly proportional to the magnitude of acceleration or applied force experienced by the accelerometer at every instant.⁽⁷⁾ The components of a piezoelectric accelerometer are shown in Figure 2.⁽⁷⁾

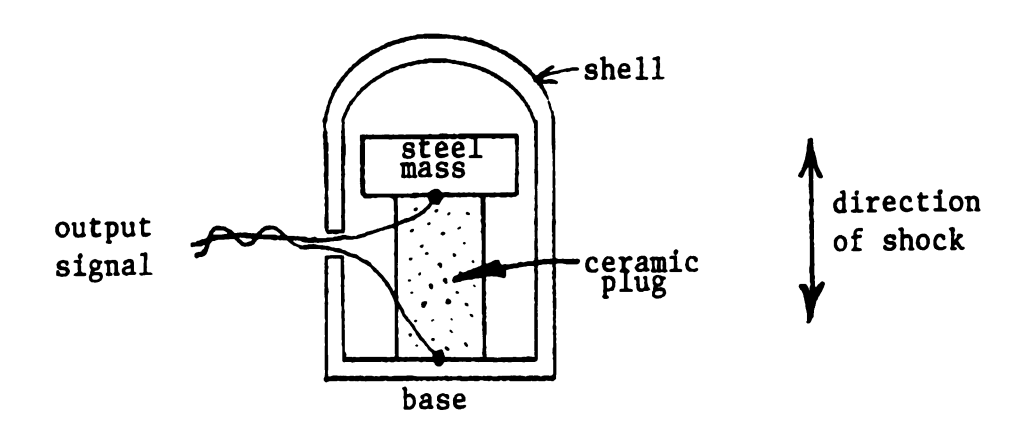


FIGURE 2: Inside a Piezoelectric Accelerometer

The piezoelectric effect describes the ability of certain crystalline materials to produce an electric charge under mechanical loading, and the ability to

harness and amplify the electric charge has allowed piezoelectric accelerometers to become a standard sensor for measuring acceleration in the packaging industry.^(7,18) The crystalline materials used as the spring of the spring mass system are most commonly quartz or ceramic. Quartz is naturally piezoelectric, but ceramic materials are forced to become piezoelectric by a polarization process that aligns the electric dipoles.⁽¹⁵⁾ Although ceramic is commonly found in piezoelectric accelerometers, quartz is generally regarded as the preferred material due to its stress limit, temperature resistance, high rigidity, and insensitivity to static charge when compared to crystalline ceramics.⁽¹⁵⁾

The method used to harness and amplify the electric signal determines the type of piezoelectric accelerometer. The two categories are high-impedance, also known as charge mode, or low-impedance, also known as voltage mode. Low-impedance accelerometers utilize a charge to voltage converter called a coupler, which amplifies the signal generated by the accelerometer so that it can be accurately measured. The use of a coupler differentiates a low-impedance accelerometer from a high-impedance accelerometer that does not contain signal conditioning. Both high and low impedance accelerometers require an external power source, coaxial cables to carry the charge signal, and software to collect, display, and analyze the output. The use of a coupler differentiates a low-impedance accelerometer that does not contain signal conditioning. Both high and low impedance accelerometers require an external power source, coaxial cables to carry the charge signal, and software to collect, display, and analyze the output.

1.2 PERFORMANCE CHARACTERISTICS

Accelerometers can be manufactured for specific applications that require certain performance characteristics. Characteristics generally used to describe piezoelectric accelerometers are, among others, amplitude range, temperature range, transverse sensitivity, weight, frequency response, and sensitivity. The amplitude range for accelerometers used in the packaging industry is from 0 to 500 g's. The accelerometer can perform at temperatures ranging from -400°F to 1400°F. The transverse sensitivity is usually less than 5%. The weight of the accelerometer is commonly 1 -15 grams. The accuracy is good at frequencies between 1-20,000 Hz, and the sensitivity is usually between 1-100 mV/g.⁽⁷⁾
Amplitude and temperature range, as well as the weight, are all characteristics that do not change during use. Transverse sensitivity, frequency response, and sensitivity degrade throughout use and require frequent reevaluation.

Accelerometers used in the packaging industry are designed with either single axis or tri-axial measurement capabilities. Single axis accelerometers measure only the change in acceleration in one direction, while tri-axial accelerometers can measure the change in acceleration on three axes. Tri-axial accelerometers are commonly used in the distribution environment where the direction of shock is random, whereas single axis accelerometers are more common on shock and vibration laboratory equipment where the direction of shock is known and controlled. Although there are many factors, the environment, either controlled or random, is the principle characteristic that differentiates between the need for a single or tri-axial accelerometer.

Transverse sensitivity of an accelerometer is caused by the misalignment of parts during manufacturing. (16) It can be described as any output caused by motion that is not along the axis of the accelerometer, and it can have a notable effect on the measured results. (7,16) The transverse sensitivity of a piezoelectric accelerometer designed for use in the packaging industry is usually guaranteed by design of the manufacturer to be no greater than 5% of the accelerometers sensitivity. (16) Although transverse sensitivity is generally regarded to have a negligible effect on measurement outputs, it is an important characteristic that is unique for each device and should be taken into account when mounting the accelerometer and analyzing the data.

The most important characteristic when measuring shock is the sensitivity of the accelerometer. The sensitivity of a piezoelectric accelerometer is the ratio of output voltage to its acceleration in g's (1 g is the acceleration in a free fall, 386.4 in/s²). The sensitivity allows for conversion of the voltage output produced by the accelerometer to its corresponding acceleration.⁽⁷⁾ As can be understood, the importance of a correct value of sensitivity is second to none in the collection of accurate data.

1.3 SYSTEM SET-UP

The setup for generating, recording, and analyzing a shock pulse from a low impedance piezoelectric accelerometer contains coaxial cables, a charge amplifier, and a data acquisition system.⁽⁷⁾ An example of a typical set up is shown below in Figure 3.⁽⁷⁾ The accelerometer is mounted to the test structure, either adhesively or by a mounting stud, and attached to coaxial cables. The coaxial cables carry the signal generated by the accelerometer to the charge amplifier, which amplifies the charge, and the amplified charge is then carried by coaxial cables to the data acquisition system; resulting in a displayed shock pulse.

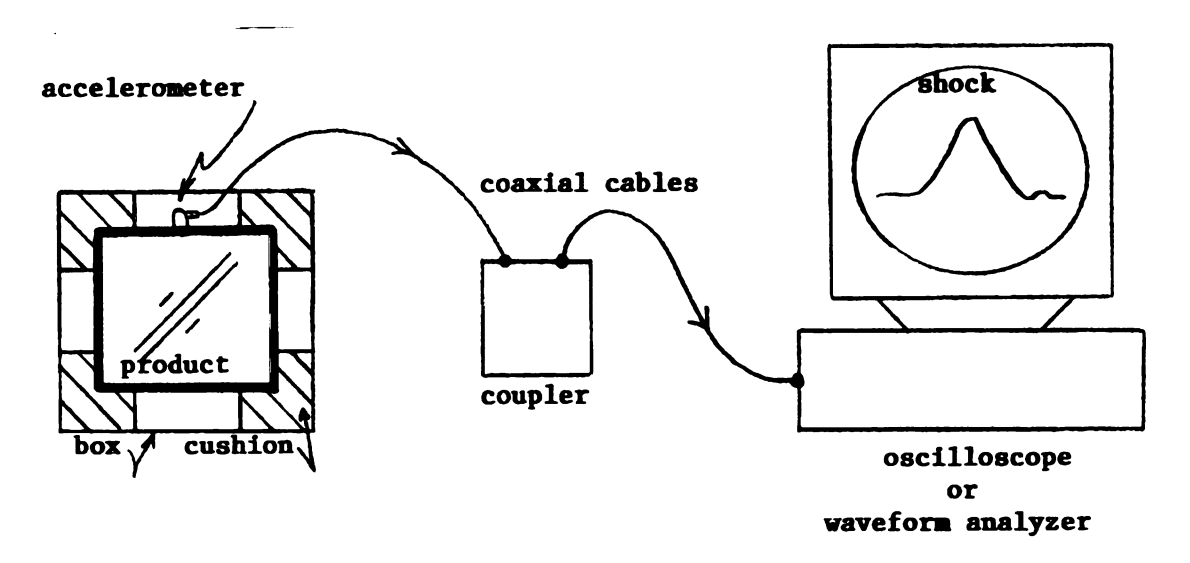


FIGURE 3: Typical Accelerometer System Setup

1.3.1 MOUNTING TECHNIQUES

The technique used to mount the accelerometer to the test structure is as important as the selection of the accelerometer in many applications. (13) If the motion of the test structure is not transmitted accurately to the accelerometer the acceleration cannot be accurately measured. (13) The two most common methods of mounting an accelerometer are a threaded mounting stud or an adhesive, but other methods, such as magnetic adapters, are also used. The type of accelerometer and the surface of the test structure are the determining factors between the use of a threaded mounting stud or an adhesive. Regardless of the method used, the surface must first be clean and smooth to ensure the flush mating of the accelerometer to a flat surface.

The threaded mounting stud is the industry preferred method because it provides higher transmissibility between the accelerometer and the test structure than any other method. (13) Also, the thread size, length of the stud, and the applied torque are all provided by the manufacturer and ensure repeatability in the installation. (13) However, in the packaging industry most packages are not manufactured with a threaded hole for the stud and modification of the mounting surface is not acceptable.

Adhesives are used to mount the accelerometer when modification of the surface is unacceptable. An adhesive material (i.e. hot glue, double sided tape, wax, etc.) is applied at a uniform thickness between the test structure and the accelerometer. The thickness of the adhesive is critical in the performance of the measurements, and the highest transmissibility of motion is achieved with a

minimal amount of adhesive.⁽¹⁴⁾ Temperature, stiffness of the cured adhesive, weight of the accelerometer, and the range of expected amplitude are factors that determine the type of adhesive used for a specific application. However, the primary concern of adhesively mounting an accelerometer is ensuring the uniformity of the adhesive.⁽¹⁴⁾ If the thickness of the adhesive is not uniform the accelerometer may not be flush with the mounting surface. According to Texas Instruments, mounting a piezoelectric accelerometer with a ten degree tilt from the direction of shock will result in the accelerometer measuring only 99% of the total g's experienced by the test structure.⁽¹⁾

1.3.2 SHOCK PULSE INFORMATION

The data acquisition system displays the signal generated by the accelerometer as a shock pulse, which is a graph of instantaneous deceleration versus time. An example is shown below in Figure 4.

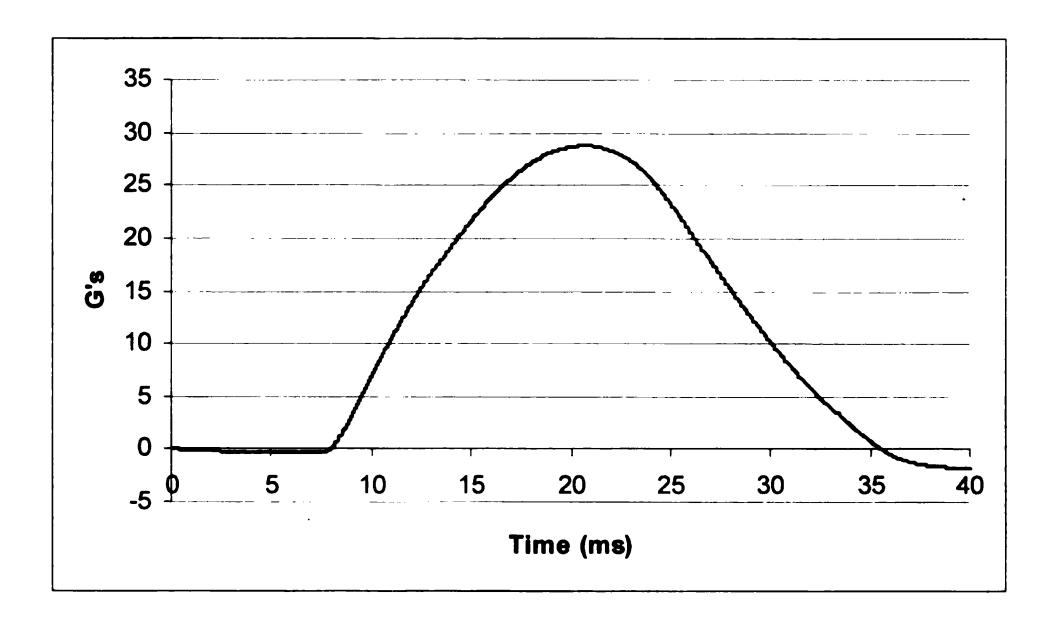


FIGURE 4: Half-Sine Wave Shock Pulse

The shock pulse gives information regarding the peak deceleration (height of the pulse), the shock duration (width of the pulse), and the change in velocity (area under the pulse). In Figure 4, the peak deceleration is equal to approximately 28 g's, the shock duration is 27 ms, and the change in velocity is approximately equal to 185 in/sec. The peak deceleration, or peak-G, and the change in velocity, or ΔV , of a shock pulse are directly proportional to the sensitivity of the accelerometer. The sensitivity of an accelerometer is expressed in mV/g, and is used by the data acquisition system to convert the voltage signal generated by the accelerometer into acceleration in g's. The duration of the

shock pulse does not require conversion, and, in turn, is not affected by the sensitivity. An incorrect sensitivity will result in an inaccurate voltage to g's conversion, and, ultimately, an inaccurate change in velocity over the duration of shock.

1.3.3 FILTERING

A shock pulse is not always as "clean" as the example shown in Figure 4. For noisy shocks, computer software is used to filter the pulse, making it more readable.⁽⁷⁾ A low pass frequency is used to remove high frequency noise. The correct filter frequency can be determined automatically by the software, manually by the user, or can be left out altogether.

An unfiltered shock pulse will be displayed with many peaks and valleys, referred to as noise, that make the results difficult to interpret, especially by people unfamiliar with dynamic testing. An example of an unfiltered shock pulse is shown in Figure 5. Although the shock pulse is difficult to interpret by the human eye, software automatically calculates the peak-G, duration, and the ΔV of the shock pulse.

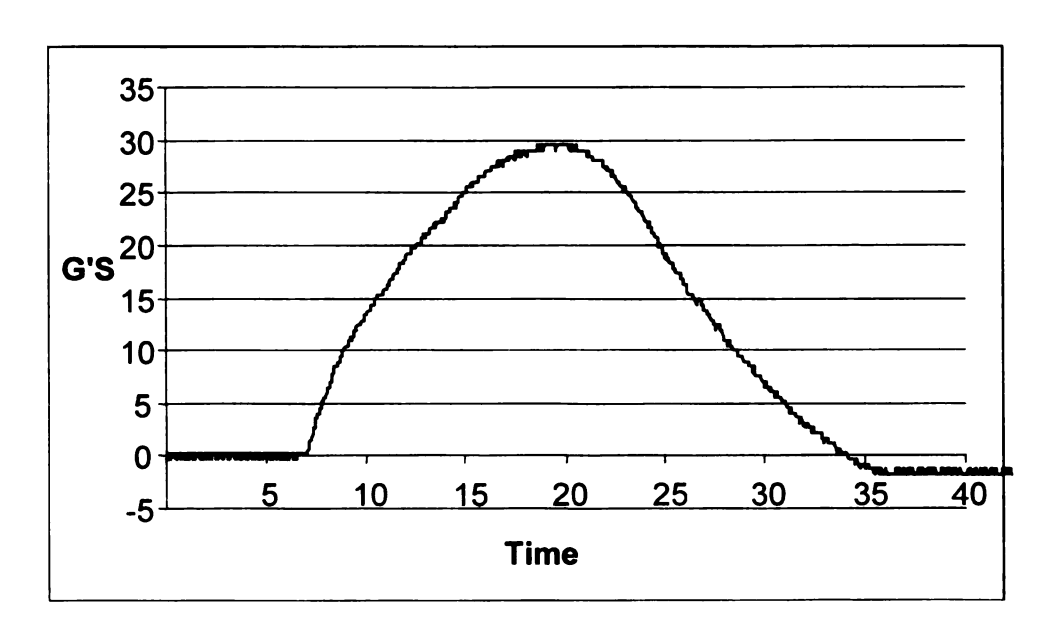


FIGURE 5: Unfiltered Shock Pulse

The automatic filter "filters" out the high frequency "noise" and allows the low frequency signals to pass without modification. (11) It will result in a shock pulse that is free from noise and almost impossible to misinterpret. However, distortion of the measured shock duration and peak-G must be considered. Figure 6 below is the automatically filtered version of Figure 5 above. Figure 5 displays a peak deceleration of 29.5 g's, shock duration of 28 ms, and a change in velocity approximately equal to 200 in/sec, while Figure 6 displays a peak deceleration of 28 g's, shock duration of 27 ms, and a change in velocity of 185 in/sec.

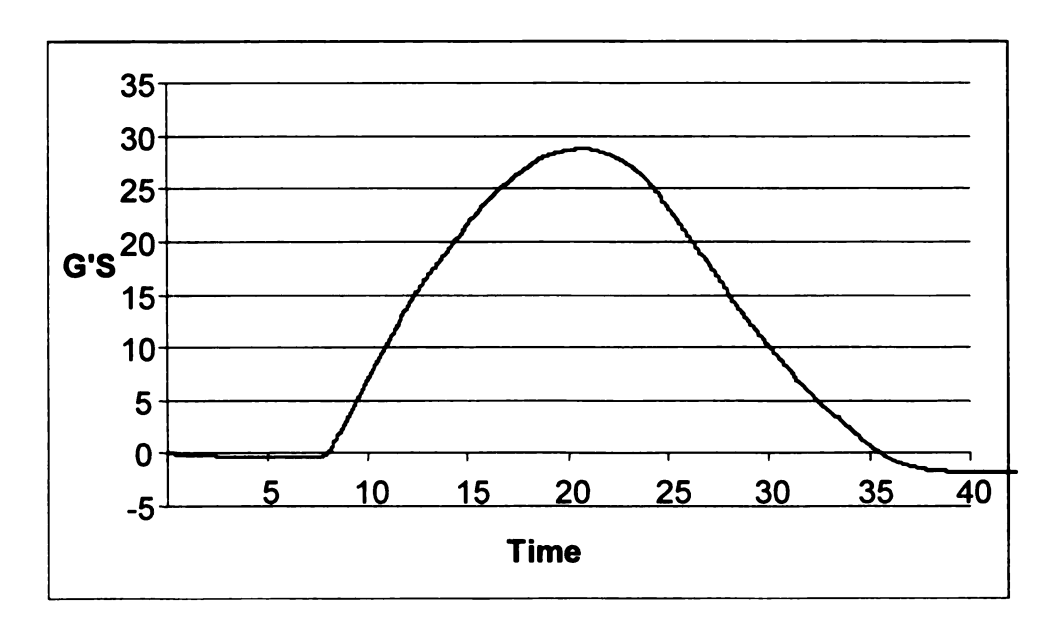


FIGURE 6: Automatically Filtered Shock Pulse

A shock pulse that is manually filtered can also be free from noise, but the accuracy of the results is dependent on the filter frequency used. In order to avoid distortion of the waveform, the frequency should be at least five times as great as the pulse frequency. The pulse frequency is determined by considering

the duration of the shock pulse to be half the period of a sine wave. Multiplying it by two results in the period of a full-sine wave. The reciprocal of the period gives the fundamental frequency of the shock pulse. Five times the fundamental frequency will give the filter frequency. In Figure 6, the filter frequency would be $(1/2(.027))^*5$ which equals 92.59 Hz. Manually calculating the filter frequency of the shock pulse tends to lead to over-filtering, and requires frequent reevaluation of the shock pulse duration for each application. See Appendix A for the manual filter frequency used in trials.

1.4 CALIBRATION TECHNIQUES

Accelerometer sensitivity is known to degrade over time and use, and, as suggested by many sources, should be recalibrated every 6-12 months to ensure the correct signal output.

The calibration of an accelerometer is done to accurately determine the sensitivity of the accelerometer, and to define a degree of confidence in the measurements. (4) Methods of calibration can be split into two broad segments, absolute or comparison. Absolute calibration of an accelerometer calculates the accelerometer sensitivity without the use of a working standard, or reference accelerometer, while comparison calibration compares the results of a reference accelerometer with the test accelerometer. (6,20)

Calibration by comparison uses a reference accelerometer to calculate the difference in output, but relies on absolute calibration methods to frequently calibrate the reference accelerometer. The test accelerometer is mounted alongside the calibrated reference accelerometer on a test structure and is submitted to either shock or vibration in order to compare the outputs. (6,20) Methods of comparison calibration can be easily preformed as long as the sensitivity of a reference accelerometer is known, but the accuracy of the data is directly related to the ability of the absolute calibration method to calculate the sensitivity of the reference standard.

Commercially acceptable reference accelerometers from the National Institute of Standards and Technology (NIST) that have been calibrated by vibratory methods using reciprocity or laser interferometry can be obtained. (4)

The NIST provides a reference accelerometer that is traceable back to an absolute physical standard and gives comparison calibration methods commercial value.

Reciprocity and laser interferometry are two independent and absolute methods of calibration that were designed by the NIST to eliminate uncertainty in the determination of accelerometer sensitivity. The reciprocity method exposes the test accelerometer and a set of standard reference masses to controlled low vibratory frequencies, and measures their current transfer admittance to calculate the sensitivity. The laser interferometry technique, also known as the fringe counting method, uses the wavelength of a laser as a standard for measure of displacement. The accelerometer is exposed to vibration and an ideal sinusoidal excitation is assumed. The displacement of the accelerometer, as compared to the laser, combined with the frequency will allow the calculation of accelerometer sensitivity.

True confidence in methods of vibratory calibration, either absolute or comparison, can only be achieved if the accelerometer sensitivity is calibrated over the entire specified frequency range. (4) Calibrating the accelerometer over an entire frequency range will ensure that sensitivity degradation is not present at higher frequencies. (4)

Reciprocity and laser interferometry calibrated reference accelerometers are also used as comparison accelerometers in shock mode calibration by the NIST.⁽³⁾ The relationship of an accelerometer calibrated under vibration and its performance when submitted to shock is assumed to be comparable, but the

vibratory calibration of an accelerometer, whose primary use is in shock applications, could result in sensitivity degradation of the accelerometer.

Accelerometers are modeled towards specific applications, but calibration methods, especially absolute methods, do not follow this same pattern of design.

One absolute method of calibration that is not performed under vibration is a gravimetric calibration system. The gravimetric calibration system provided by PCB Electronics, Inc. is a method that submits the test accelerometer to a period of free fall where the acceleration is known to be 1g.⁽²⁾ The method uses the 1g step combined with the measured voltage to calculate the sensitivity.⁽²⁾ The sensitivity is calculated using 1g, but in the packaging industry, accelerations of this magnitude are infrequent.

1.5 COST

In the packaging industry, acceleration sensing and measuring systems minimize costs associated with the design of protective packaging by reducing packaging materials, product damage, and package development time. Cost reduction and technological advancements have promoted the growth of the acceleration sensing industry, and as it grows, the cost of piezoelectric accelerometers continues to decrease.

Piezoelectric accelerometers used in the packaging industry vary in price from \$350 to \$500, depending on the performance characteristics. Coaxial cable to carry and protect the accelerometer signal from outside noise is generally sold for \$20-\$50 per 10 feet of cable. The system coupler, which is used to amplify the signal, ranges in price from \$200-\$300, and the shock response hardware and software, used to display and analyze the signal, ranges from \$7000 to \$12,000 depending on the complexity of the application. For the simplest of applications, the total cost of a low impedance acceleration sensing system will cost approximately \$8000, and that does not include the recalibration of the accelerometer. The calibration of accelerometer sensitivity can cost up to \$100, excluding the cost of shipment and the time involved.

1.6 OBJECTIVES

Current methods of calibration rely on additional equipment to provide scaling values for the calibration of an accelerometer, and when the equipment is not controlled properly variances can occur in measurements. (4) The Modal Shop, Inc., a PCB Group Company, states that uncertainties on the order of 3% can be expected in calibrations performed by separate calibration laboratories. (4) The proposed method is an alternative solution to current methods of calibration that can be costly and unreliable.

The method is designed to be an in-house supplement to packaging laboratory equipment that is inexpensive to manufacture and cost effective to implement. The method is not designed to alter the accelerometer sensitivity, but rather to calculate the current sensitivity of the device. Actually altering the accelerometer sensitivity to a desired value is not necessary to generate accurate results.

Within the industry, calibration does not mean that the accelerometer is actually adjusted to recreate its original sensitivity. Calibration is done by physically adjusting the electronics of the coupler to alter the sensitivity of the accelerometer to a desired value. The coupler is a device that amplifies the signal generated from the accelerometer by the magnitude of its sensitivity (the ratio of output voltage to its acceleration in g's). The industry does not calibrate the accelerometer, in the usual sense of the word, but, instead, the current sensitivity of the accelerometer is calculated and the coupler is adjusted to compensate for any change in sensitivity. The sensitivity is thus accurate for the

entire system and not just the accelerometer, and any change to system will alter the sensitivity of the accelerometer.

The objectives of this thesis are:

- To develop a simple, inexpensive, and accurate method of absolute shock mode calibration for piezoelectric accelerometers by utilizing a hammer with frictionless bearings and a video recording system.
- To develop a method of absolute shock mode calibration that can be used throughout a range of g-levels and shock durations commonly seen in the packaging industry.
- To build and test the device used in the method and validate its performance.
- To validate the insensitivity of the absolute shock mode calibration method to signal filtering methods.
- To validate the insensitivity of the absolute shock mode calibration method to experimental errors.

1.7 CONCEPT

The absolute shock calibration of an accelerometer can be performed by measuring the change in velocity resulting from the impact of an accelerometer, and comparing it to what the shock pulse says. The shock pulse, shown in Figure 7, gives information regarding the peak deceleration (peak-G), the shock duration (ms), and the change in velocity (ΔV) . The change in velocity is the area enclosed by the shock pulse. The area is calculated by the data acquisition system by dividing the curve into thin rectangles and then taking the sum of the thin rectangles to equal the area enclosed by the shock pulse.

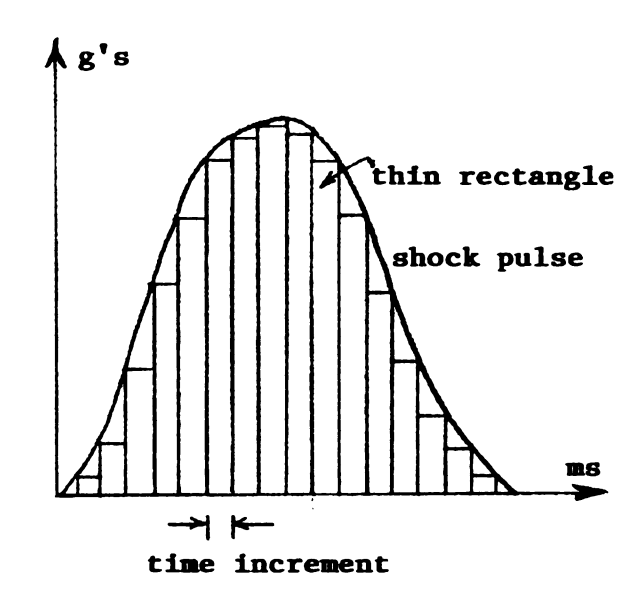


FIGURE 7: Half-Sine Wave Shock Pulse - Area

The change in velocity of the shock pulse, as compared to the peak-G and duration, is relatively insensitive to filtering; meaning that, regardless of the filter frequency chosen, the area enclosed by the shock pulse will be unchanged.

Signal filtering averages out the peaks and valleys of a shock pulse and results in a smooth shock pulse that, although different in appearance, is identical in area

to an unfiltered shock pulse. It also provides the capability to compare the area under the curve to a known, independently calculated, value. The peak-G and duration of the shock pulse are impossible to independently calculate with the materials and procedures described in this method.

In a situation where an object is dropped from some height onto on impact surface, the change in velocity can be determined by adding the velocity of impact (V_i) to the rebound velocity (V_r) .

$$\Delta V_{\text{actual}} = V_i + V_r \tag{1}$$

Assuming no wind resistance, the impact and rebound velocity can be related to the drop and rebound heights, respectively, by the following equations.⁽⁷⁾

$$V_i = (2gh_d)^{\Lambda^{1/2}} \tag{2}$$

$$V_{r} = (2gh_{r})^{\Lambda^{1/2}}$$
 (3)

where

g = Acceleration due to gravity (386.4 in/s²)

h_d = Drop height (inches)

 h_r = Rebound height (inches)

Equations 2 and 3 show that the velocity change is dependent only on the drop and rebound heights of an object in free fall, and this is shown in equation 4 below.

$$\Delta V_{\text{actual}} = (2gh_{\text{d}})^{\Lambda^{1/2}} + (2gh_{\text{f}})^{\Lambda^{1/2}}$$
(4)

In a controlled experiment, the drop height of the object is known, but the rebound height is dependent on many factors, primarily the impact surface, and

so it must be measured to accurately determine the change in velocity. The development of a consistent, repeatable, method of measuring the rebound height, while maintaining minimal friction and wind resistance, is the key to mathematically calculating the actual ΔV and eventually the sensitivity of the accelerometer. One way to accomplish this is to videotape the drop. By videotaping the drop, the slow motion replay of the drop can be viewed and the rebound height can be measured in reference to a background scale. The correct sensitivity of the accelerometer is the mv/g ratio that makes ΔV_{pulse} equal to ΔV_{actual} .

Developing a repeatable method of this stature is difficult to do experimentally. A cushion tester, common to packaging laboratories, provides all the necessary requirements for this method, minus the absence of friction. The bars used as the guides to the platen are often unparallel and can create a slight ratcheting motion by the platen during its downward acceleration. Even if the bars are assumed to be perfectly parallel, the sliding motion of the platen through the bars creates frictional forces if not properly lubricated. Thus, the cushion tester cannot be guaranteed to provide a frictionless system, and the need for a frictionless system is realized.

CHAPTER 2

MATERIALS AND METHODS

2.1 DESRIPTION OF CALIBRATION DEVICE

The frictional forces of a rotational mechanism are much less than a mechanism with a sliding motion.⁽¹⁰⁾ A hammer with an axle through the handle accomplishes this and is shown in Figures 8 and 9.

Figure 8 illustrates the method that will be used to capture a shock pulse. The accelerometer is attached to the head of the hammer and the hammer is allowed to drop downward from a vertical position to impact a cushioned surface, thus generating a shock pulse. Figure 9 shows the hammer inverted. This setup will be used to determine the natural frequency of the hammer acting as a pendulum. This information will eventually be used to calculate the actual velocity change of the hammer head.

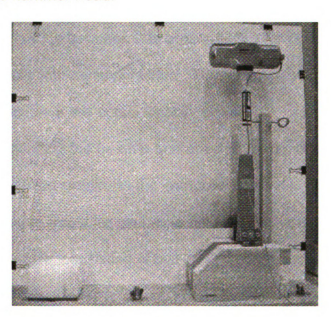


FIGURE 8: Absolute Calibration Device - Shock

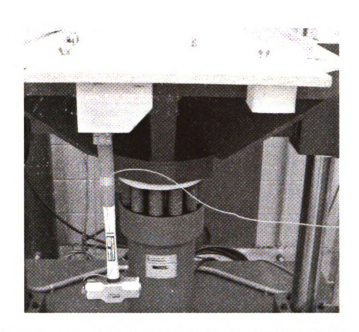


FIGURE 9: Absolute Calibration Device - Natural Frequency

The accelerometer is adhesively mounted on top of the horizontal axes of the steel head of the hammer. The hammer has a graphite handle that measures approximately 14 ¼" in length and the steel head of the hammer is approximately 2" in diameter and 6 ¼" in height. The end of the hammer handle, opposite from the head of the hammer, has been modified to fit bearings that allow the handle to rotate with minimal friction. The absence of friction is essential for the calculation of the actual velocity change.

The hammer, including the bearing and accelerometer, is supported by a wood structure that provides stability to the components, and is manufactured to allow the hammer to rotate freely, as well as to eliminate variance in the angle of impact. The wood structure, consisting of two 2 X 4 boards cut to 6" in length and separated by 2", is attached to a plywood base that is bolted to a shock

machine. An illustration of the bearings and structure is given in Figure 10 helow

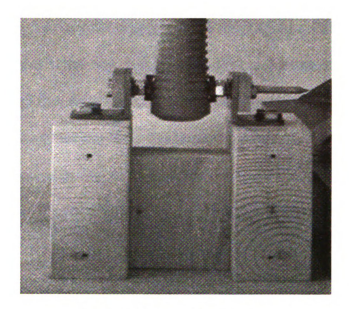


FIGURE 10: Bearings

The impact surface is attached to the wooden platform equidistant from the bearing as the steel head of the hammer, and the height was modified to make the handle horizontal at impact. The impact surfaces used in the verification of the calibration method were rubber (rubber ball), compressed air (tennis ball), and a 2 pcf (pounds per cubic foot) foam cushion. The radius of the rubber ball was 1 1/8", the tennis ball was 1 3/16", and the 2 pcf foam cushion stood 2 ½" tall

The background scale shows the angle of the handle after it rebounds. It was constructed using the ArtiosCAD software program, etched on to a sheet of paperboard, and attached to a wooden backing. The backing was then attached to the wooden platform to provide stability for the scale, as well as for

repeatability in the scale mounting and measured results. The scale is designed to provide measurement capabilities of the rotating hammer from 0-90 degrees at one degree of accuracy. An arrowed tip was also manufactured and adhered horizontally on to the end of the hammer. The tip provides ease of use in precisely recording the rebound angle of the horizontal axis of the hammer. When the head of the hammer contacts the impact surface the handle is horizontal and the scale reads 0°. An illustration is shown below in Figure 11.



FIGURE 11: Absolute Calibration Device - Angle of Impact

The last component, not including the accelerometer, is a camera with video recording capabilities of at least thirty frames per second (30 fps). The rebound height of the hammer, which results from impact with the cushioned surface, is determined by the angle of rebound, and is a key measurement required for calibration. Video recording captures the angle of rebound for the hammer. The height of the camera remains constant throughout the video

recording of each impact surface by the use of a tripod. The tripod is used for camera stability, but also provides repeatability in the recorded results.

The entire calibration device was bolted, both upright and inverted, to the table of a shock machine. Shock machines are common to packaging laboratories. The shock machine is a seismic mass that, when bolted to, provides stability to the test structure for both parts of testing. Although the shock machine is convenient to use, any rigid structure that can support the weight of the calibration device is acceptable for use, including the floor during shock applications.

The absolute calibration device is inexpensive to manufacture, and the materials used are common to any laboratory. Manufacturing the test structure out of wood preserves a low cost for development, and it also allows the test structure to be tailored towards specific testing environments. As long as rotational friction is minimized and the correct method is followed, the materials used for the test structure prove to be insignificant to the results.

2.2 METHOD OF USE

The absolute shock calibration method for a piezoelectric accelerometer consists of two separate parts that are equally important to calculate the sensitivity of the accelerometer. The first method is performed to determine the natural frequency of the hammer acting as a pendulum, and the second method is executed to capture the change in velocity of the accelerometer when subjected to shock.

2.2.1 NATURAL FREQUENCY

A pendulum has a natural frequency that is measured in cycles per second (cps).⁽⁷⁾ A cycle is defined to be one complete "back and forth" motion by the pendulum.

The method used to determine the natural frequency of the pendulum (hammer including accelerometer) is illustrated in Figure 9 above. First, the scale is removed and the plywood base is flipped over and bolted onto the table of the shock machine. The hammer including the accelerometer is then hanging upside down and free to rotate. The hammer is manually set into motion, upon which it "swings" back and forth, and the cycles per second are counted and recorded as its natural frequency.

Determining the natural frequency of the pendulum is an integral step for calibration, and should be consistently re-evaluated, especially if the set up is altered, to ensure correct results.

2.2.2 CHANGE IN VELOCITY

The second part in the absolute shock calibration method is to determine the change in velocity, both from the shock pulse and, independently, from the measured rebound angle.

The wooden platform is positioned "upright" and is bolted to the table.

Next, the background scale and the desired impact surface are placed on the wooden platform. The hammer is then positioned, by the use of a prop shown in Figure 12, to stand perpendicular to the wooden platform. The hammer is positioned at a 90-degree angle in order to maintain a standard drop height, and to allow the hammer to be released from rest; meaning its' initial velocity is equal to zero.



FIGURE 12: Absolute Calibration Device - Release Angle

The data acquisition system is then prepared to capture a shock pulse by inputting the sensitivity of the accelerometer, choosing the filtering method, and selecting the axis of measurement. Next the camera is situated on the tripod and the recording begins prior to the hammer being set into motion.

The hammer tips over and impacts the cushioned surface. The hammer strikes the cushion and rebounds off the surface. The upward rotation is then captured by the video recording, after which the maximum rebound angle is determined and recorded in reference to the background scale.

The shock pulse from the impact is displayed by the data acquisition system. The software then calculates the area under the shock pulse. This area represents the change in velocity according to the accelerometer. Comparison to the actual change in velocity (see theory below) shows whether the accelerometer sensitivity is correct or not.

2.3 THEORY

The principle of conservation of energy states that energy may be transformed from one kind to another, but it cannot be created or destroyed; the total energy is constant.⁽¹⁰⁾ In the shock calibration method the hammer is released from rest to promote a transformation from potential to kinetic energy.

The potential energy of the system can be written, with respect to the angle θ , as:⁽¹⁰⁾

$$PE = mg(a*sin \theta)$$
 (6)

where

m = mass of hammer and accelerometer together

a = distance from the axle to the center of gravity of the hammer

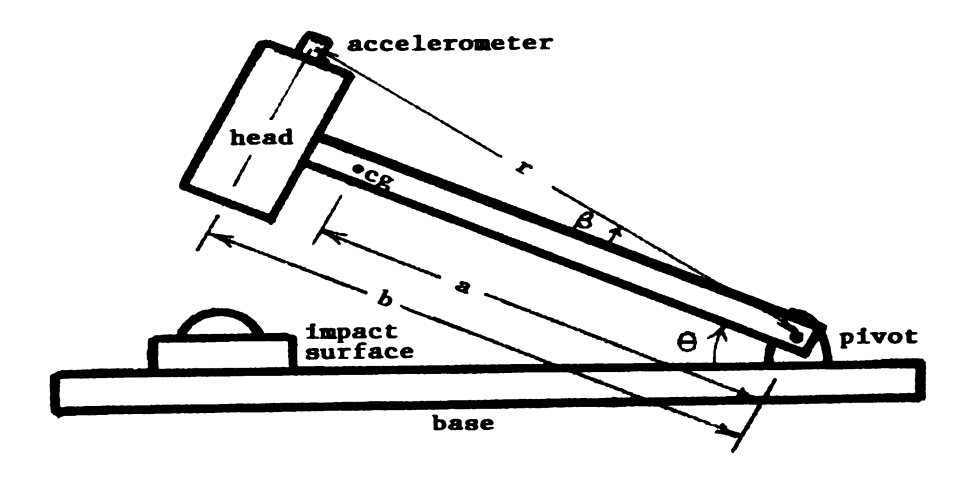


FIGURE 13: Variables Associated with the Theory

The kinetic energy (KE) of a rigid body can be written as a function of its rotational inertia, also known as its moment of inertia, and its angular speed.⁽¹⁰⁾
The equation used to calculate the KE is

$$KE = \frac{1}{2}I_{p}\omega^{2} \tag{7}$$

where

 I_p = moment of inertia about axle

 ω = angular velocity

Conservation of energy can then be written as a transformation from potential to kinetic energy (KE = PE) by equation 8 below:

$$mg(a*\sin\theta) = \frac{1}{2}I_p\omega^2 \tag{8}$$

Solving equation 8 for angular velocity gives

$$\omega = [(2^*m^*g^*a^*\sin\theta)/(I_p)]^{1/2}$$
 (9)

The velocity of an object executing circular motion is always tangent to the circle in the direction of motion. The accelerometer mounted on top of the hammer is moving in a circle of radius r (see Figure 13), so its velocity at the point of impact is $v = \omega r$. However, the accelerometer only senses motion along its axis, which is in the vertical direction of impact, and, therefore, the velocity of the accelerometer along the direction of its sensing axis is equal to:

$$V_{v} = V * \cos \beta \tag{10}$$

where

V = velocity tangent to circle = ωr

 β = angle between tangent velocity and y-axis

The angle β is shown in Figure 13. Equation 10 can therefore be written as in equation 11 below:

$$V_{v} = V * (b/r) \tag{11}$$

where

r = distance from the axle to the accelerometer

b = distance from axle to the vertical axis of the accelerometer

The velocity of the accelerometer is the product of the angular velocity and the radius of the circle. After substitution,

$$V_v = (\omega * r)(b/r) = \omega * b$$
 (12)

or, after combining with equation 9.

$$V_{v} = b * [(2*m*g*a*sin \theta)/(I_{p})]^{1/2}$$
 (13)

The change in velocity of the hammer traveling in a uniform circular motion can be calculated by combining equations 4 and 13, and this combination is illustrated in equation 14.

$$\Delta V_{actual} = b * [(2*m*g*a)/(I_p)]^{1/2} {[(\sin \theta_d)^{1/2} + (\sin \theta_r)^{1/2}]}$$
 (14)

where $\sin\theta_d$ and $\sin\theta_r$ are equal to the drop and rebound angles, respectively. Equation 14 applies only to an object that, after being dropped, travels in a uniform circular motion (i.e. hammer rotating on an axis). The equation is also only valid when minimal frictional forces are acting against the rotation of the device.

All variables in equation 14 are easily measured with the information at hand except for the moment of inertia. Calculating the moment of inertia requires further quantification, which, as it turns out, can be related to the natural frequency of the device.

2.3.1 Simple Harmonic Motion of a Pendulum

Newton's law applied to the motion of a pendulum states that

$$\tau = I_p * \alpha \tag{16}$$

where

 τ = torque about a fixed axis of rotation

 α = angular acceleration

The torque is determined by multiplying the force (F) acting on the pendulum by its' distance from the rotational axis. (10) The force applied to the pendulum is its own weight, and acts at the center of gravity of the body. The distance of the center of gravity from the axis of rotation is $a^*\sin \phi$, where ϕ is the angle between the handle and the vertical. So,

$$-mg^*a^*sin \phi = I_p * \alpha \tag{17}$$

At small amplitudes of oscillation the sine of the angular displacement (ϕ) of motion in radians is approximately equal to the angle itself, in radians. Thus

$$\sin \phi \cong \phi$$
 (18)

which results in equation 17 being re-written as

$$-mg^*a^*\phi = I_p * \alpha \tag{19}$$

The angular acceleration (α) is the second derivative of the angular displacement ϕ . Substituting gives the equation of motion for a simple harmonic oscillator, shown in equation 20. This is a differential equation that determines the angular displacement as a function of time

$$(d^2\phi/dt^2) + (mga/I_p) \phi = 0$$
 (20)

Solving the differential equation of motion (equation 20) gives

$$\phi(t) = A * \cos(\omega t) \tag{21}$$

where A is the amplitude of motion, and

$$\omega = ((m^*g^*a)/I_p)^{\Lambda^{1/2}}$$
 (22)

The period is

$$T = 2\pi/\omega \tag{23}$$

The natural frequency (f_n) is the number of cycles per unit time, and thus the period of motion is related to the natural frequency by taking its reciprocal.

$$f_0 = 1/T = \omega/2\pi \tag{24}$$

Combining equations 22 and 24 results in:

$$I_p = (m^*g^*a) / ((2\pi f_p)^{\Lambda^2}$$
 (25)

Substituting this into equation 14 allows the change in velocity to be calculated in terms of the natural frequency, without having to know its moment of inertia. Substituting equation 25 into equation 14 results in

$$\Delta V_{\text{actual}} = b * 2\pi f_n * (2)^{1/2} \{ [(\sin \theta_d)^{1/2} + (\sin \theta_r)^{1/2}] \}$$
 (26)

The change in velocity experienced by the accelerometer in the direction of its axis can now be determined by measuring the natural frequency (f_n), the distance from the vertical axis of the accelerometer to the axis or rotation (b), the drop angle (θ_d), and the rebound angle (θ_r) of the hammer after maximum cushion compression.

The area under the shock pulse must match the mathematically determined change in velocity. If the two do not agree, then the sensitivity (mv/g) of the accelerometer is incorrect. The correct sensitivity can be determined as described next.

2.3.3 SENSITIVITY

The ability to mathematically calculate the actual change in velocity allows the user to compare the velocity change according to the shock pulse (given by the data acquisition system), referred to as ΔV_{pulse} , to the actual velocity change, or ΔV_{actual} . If ΔV_{pulse} does not equal ΔV_{actual} , within a range of tolerance, the sensitivity of the accelerometer is incorrect. In order to determine the actual sensitivity of the accelerometer, a correction factor is calculated by taking their ratio. The correction factor (f) is determined by the following equation:

$$f = (\Delta V_{actual} / \Delta V_{pulse})$$
 (27)

Suppose, for example, that a drop is made and the actual velocity change is calculated, using equation 26, and found to be 110 in/sec. Further suppose, the accelerometer captures a shock pulse and the data acquisition system calculates, using an assumed sensitivity of 10 mv/g for the accelerometer, the velocity change (area enclosed by the shock pulse) to be 100 in/sec. The correction factor in this case would be f = 110/100 = 1.1, meaning that the correct sensitivity of the accelerometer is really 1.1*10 mv/g = 11 mv/g. If the 11 mv/g sensitivity is now input into the data acquisition system and the shock pulse is redisplayed, it will be 10% greater in height (all g's will be increased by a factor of 1.1), and, thus, it will recalculate the velocity change to be 110 in/sec, exactly the same as the known actual velocity change.

CHAPTER 3

RESULTS

3.1 NATURAL FREQUENCY

Following the method described in Chapter 2, the natural frequency of the hammer, including accelerometer, was measured. The cycles were manually counted while a stopwatch measured the time, in seconds, that it took for the hammer to execute a given number of complete cycles. The results are given in Table 1 below:

NATURAL FREQUENCY			
Trial	Cycles	Time (sec)	Fn
1	10	11.91	0.8396
2	10	12.00	0.8333
3	10	11.92	0.8389
4	10	11.89	0.8410
5	10	11.96	0.8361
6	15	18.00	0.8333
7	15	17.86	0.8399
8	15	17.95	0.8357
9	15	17.98	0.8343
10	15	17.95	0.8357
11	30	36.08	0.8315
12	30	36.00	0.8333
13	30	35.98	0.8338
14	30	35.94	0.8347
15	30	35.98	0.8338
16	50	60.15	0.8313
17	50	59.50	0.8403
18	50	60.16	0.8311
19	50	60.00	0.8333
20	50	59.93	0.8343
21	75	90.05	0.8329
22	75	90.03	0.8331
23	75	90.07	0.8327
24	75	90.26	0.8309
25	75	90.32	0.8304
26	100	120.18	0.8321
27	100	120.25	0.8316
28	100	120.39	0.8306
29	100	120.14	0.8324
30	100	120.18	0.8321
		Average =	0.8341 cps
		Std. Dev. =	0.0030 cps

TABLE 1: Natural Frequency Results

The natural frequency was determined using a broad range of time durations in order to prove that minimal frictional forces are present in the rotation of the device. The hammer showed no deterioration in motion after 100 cycles when compared to 10 cycles, thus proving the absence of friction. The average of the individual trial results was then calculated and taken as the natural frequency.

3.2 REBOUND ANGLES

The maximum rebound angle of the hammer was identified at the point when the hammer slowed to a stop and again began to fall. The recorded image transitions from a blurry image when in motion to a sharp and clear image when it momentarily stops. The difference between the two images, blurry and clear, is illustrated below in Figures 14 and 15.

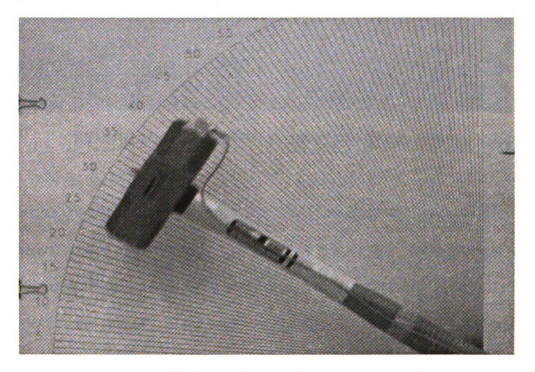


FIGURE 14: In Motion Rebound - Blurry Image

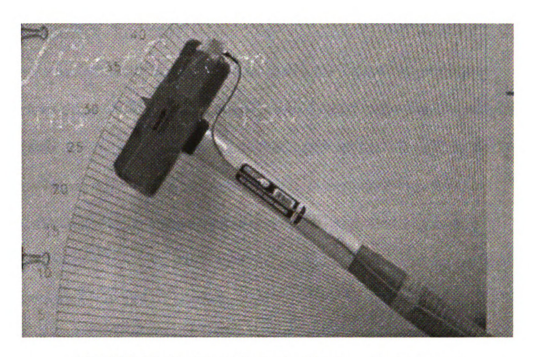


FIGURE 15: Maximum Rebound Angle - Sharp Image

Despite the precision of the video, the angle measurement system still may produce errors in measurement, but any error in the angle measurement is ultimately reduced by the power of ½ when input into equation 29. A 5% error in measurement of the rebound angle results in a 2.5% error in maximum velocity change. In one trial, assuming a 5% error in the angle, the percent error in the change in velocity was only 0.74%.

3.3 CORRECTION FACTOR

The correction factor is calculated by taking the ratio of the change in velocity values determined from the shock pulse (ΔV_{pulse}) to the actual change in velocity values determined mathematically (ΔV_{actual}) from the rebound angle. The shock pulse values were simply taken from the data acquisition system and recorded, while the rebound angle was measured through video recording. A correction factor of 1.00 would mean that ΔV_{actual} equals ΔV_{pulse} ; so the sensitivity of the accelerometer would be correct.

The performance of the calibration method was evaluated for three different impact surfaces; rubber, compressed air, and foam, as well as, for three separate methods of signal filtering; auto, none, and manual. The following results will compare the performance of the absolute shock calibration method, as determined by the correction factor, for the three impact surfaces and the three methods of signal filtering.

The performance of the method is also contingent upon beginning with an accelerometer of a known correct value of sensitivity. The accelerometer used in this research was relatively new and had been recently calibrated to a sensitivity of 10 mv/g; so the velocity change generated by the shock pulse was expected to be accurate.

For example, lets say a 90° drop was performed and a shock pulse was captured. The shock pulse was automatically filtered and the change in velocity acquired from the pulse was equal to 207.51 in/sec. During the same drop, the video recording system captured the rebound angle of the hammer. The

rebound angle equaled 58 degrees, and by substituting the angle into equation 26 gives an actual change in velocity equal to 215.23 in/sec. The correction factor between the two values, ΔV_{actual} and ΔV_{pulse} , can now be determined. Substituting into equation 27 gives a correction factor of 1.0372. Therefore, the true sensitivity of the accelerometer is 1.0372 times the sensitivity used by the data acquisition system. If the actual sensitivity is now input into the data acquisition system, the change in velocity of the shock pulse would exactly match the actual change in velocity experienced by the accelerometer. Actual experimental data of this calculation can be seen in Appendix B.

3.3.1 Impact Surfaces

The performance of the calibration method on all three impact surfaces was tested for the three filtering methods, and is listed below, beginning with the automatic filter method. The performance of the absolute shock calibration method was evaluated for three different impact surfaces in order to validate its use throughout a range of g-levels and shock durations. The results are shown in Figure 16. The rubber impact surface generates the largest peak-g's, but the shortest shock duration. The compressed air and foam cushion impact surfaces result in similar g-levels, but the duration of shock generated by the foam cushion is significantly less than the compressed air surface.

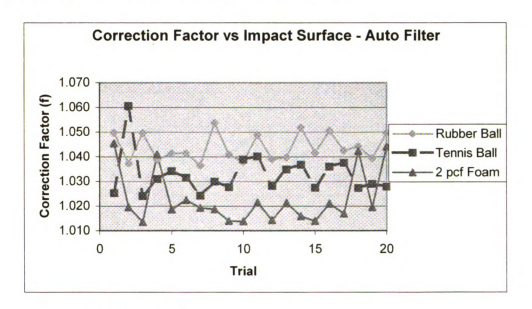


FIGURE 16: Correction Factor - Automatic Filtering

The results of the impact surface experiment for the automatic filtering method show a correction factor, regardless of impact surface, that ranges from approximately 1.0135 to 1.0606. The rubber impact surface gave the largest average correction factor, which was 1.0437, while the compressed air impact

surface was a close second with an average magnitude of 1.0327. On average, the foam impact surface gave a correction factor of 1.0228, which results in a 2.23% difference between the two values, but the results are more random and vary significantly when compared to the other surfaces. The rubber impact surface gives the most consistent results with only a 1.64% variance in the measured values, while the compressed air and foam values varied at 3.43% and 3.06%, respectively.

Next, the performance of the calibration method on the three impact surfaces without signal filtering was tested. The results are shown in Figure 17.

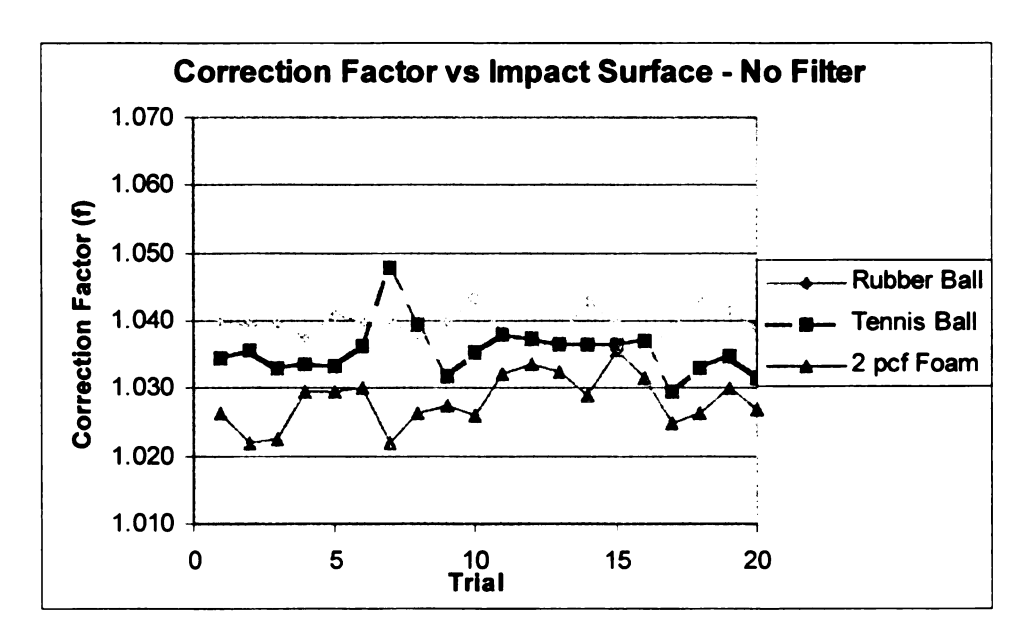


FIGURE 17: Correction Factor – No Signal Filtering

The magnitude of the correction factors for the separate impact surfaces without signal filtering has varied from the automatic filtering method, but the rubber surface still maintains the largest average correction factor of the three surfaces. The foam surface has an average correction factor of 1.0282, which, although it is greater than the automatic filtering method, is still less than the other impact

surfaces; equaling a 2.74% difference between the pulse and actual velocities. The calibration method successfully calculated the sensitivity of the accelerometer, regardless of impact surface, within a range of 4.25%, minus one outlier from the compressed air surface at 4.57%. The unfiltered results are also more consistent for each surface, with the rubber surface again being the most consistent. The rubber surface results varied only 0.75%, while the tennis ball and foam impact surfaces varied at 1.55% to 1.32%, respectively.

Lastly the results of the three impact surfaces subjected to shock with a manually input frequency, equal to five times the fundamental frequency of the shock pulse, for each corresponding surface. The results are shown in Figure 18. See Appendix A for further information regarding the filter frequencies used in the experiment.

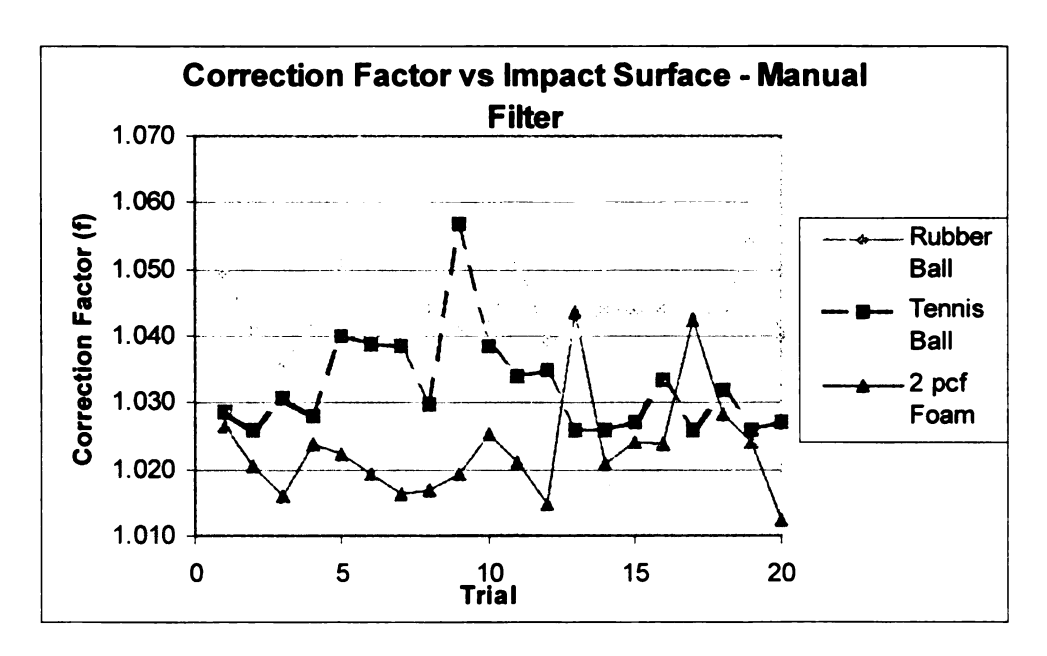


FIGURE 18: Correction Factor – Manual Signal Filtering

The impact surface results for the manual filter remain consistent with the previous filtering methods. The rubber surface, on average, maintains the

highest magnitude of correction factor, 1.0431, while the foam remains the lowest at 1.0231. The values, as expected, are much less consistent across the trials for each impact surface, but rubber is again the most consistent with a 1.72% of variance in values.

The rubber impact surface, when compared to the other impact surfaces results in the largest correction factor magnitudes, regardless of filtering method, but it does maintain the most consistent results throughout the range of trials. The impact of the absolute shock calibration device onto the rubber surface results in peak-g levels that, without filtering, average 68.25 g's; almost doubling the peak-g levels of the other impact surfaces. The g's experienced by an object being dropped are in direct correlation with the hardness of the impact surface the object was dropped on, and, as the results show, the correction factor seems to grow with the hardness of the impact surface. However, a larger correction factor does not necessarily mean inferior results. The variance between the results for the three different impact surfaces shows that there are inherent errors in the method. The error, although, is minimal and can most likely be attributed to measurement errors (i.e. mounting errors, transverse sensitivity).

The consistent results of the rubber impact surface, when compared to the other impact surfaces, were expected. The rubber impact surface is less susceptible to memory retention caused by compression then the compressed air (tennis ball) and foam (2 pcf cushion) impact surfaces.

Overall the absolute shock calibration of a piezoelectric accelerometer appears to be minimally effected by the impact surface used. The results also

show that the method of filtering affects the magnitude and consistency of the results for each impact surface. The degree of influence by each filtering method will be discussed next.

3.3.2 SIGNAL FILTERING

The absolute shock calibration of a piezoelectric accelerometer uses the change in velocity as a point of reference due to its ability to be measured independently as well as its theoretical insensitivity to signal filtering. The performance of the absolute shock calibration method was tested on each impact surface for each method of filtering; automatic, none, and manual.

The correction factor results for the rubber impact surface produced by each method of signal filtering are shown Figure 19.

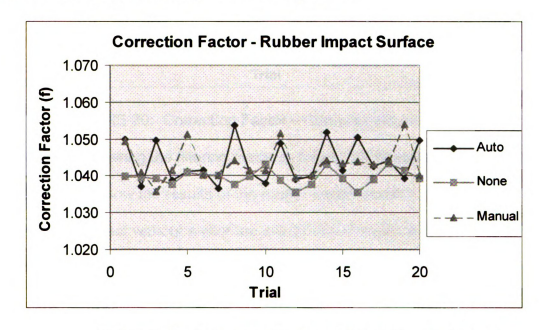


FIGURE 19: Correction Factor - Rubber Impact Surface

Figure 19 shows that, as expected, the two methods of signal filtering, auto and manual, result in a higher variance in the measured correction factor when compared to testing with no signal filtering. No signal filtering provided more consistent results with only minimum variance among trials. All three methods, although, did produce results that were in close proximity to each other, with the correction factors ranging from 1.0356 to 1.0540.

The results of the compressed air impact surface for the three methods of filtering are illustrated in Figure 20.

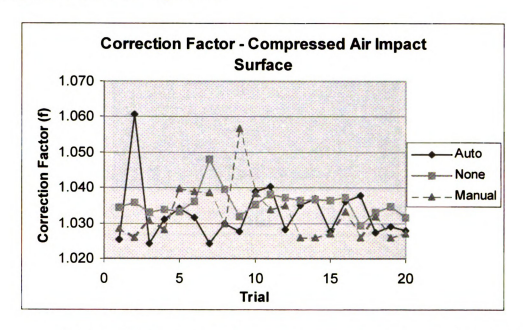


FIGURE 20: Correction Factor – Compressed Air Impact Surface
The results comparing the filtering methods for the compressed air impact
surface do not follow the results of the rubber impact surface. Although the
results from the test without a filter are still the most consistent, the range of
variance in the measured correction factor is significant for each separate
method of filtering.

Next the three filtering methods were tested on the 2 pcf foam cushion for comparison purposes. The results are shown in Figure 21.

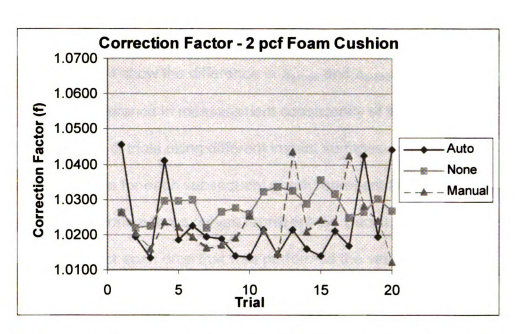


FIGURE 21: Correction Factor – 2 pcf Foam Cushion Impact Surface
The methods of filtering combined with the 2 pcf foam cushion impact surface
result in values similar to the compressed air impact surface. The absence of a
filter again produces the most consistent results, while the automatic and manual
filtering methods vary a considerable amount. The greatest correction factor
magnitudes, on average, are equal to 1.0282 and are resultant from no filtering.
The automatic and manual methods of filtering produced average correction
factors of 1.0228 and 1.0231, respectively.

The absolute shock calibration method produced the most consistent results, without using a filter, regardless of the impact surface. The automatic and manual filtering methods had significant variance among results. Although, the average correction factor values for the automatic and manual filtering methods were lower in magnitude, the inconsistency of the results creates questions in the validity of a single measured result.

3.3.3 Δ_{actual} vs Δ_{pulse}

Figures 22-24 show the difference in Δ_{actual} and Δ_{pulse} for a typical shock pulse. Note the difference in measurement consistency of the method throughout a range of trials using different impact surfaces and filtering methods. The top three curves for each subsequent graph represent the actual velocity change, while the bottom three curves represent the velocity change according to the shock pulse. For each drop that was performed the velocity change of the shock pulse and the actual velocity change of the accelerometer were measured. Even though the actual velocity change is labeled with a filtering method below, the method of filtering has no bearing on the actual velocity change. It is labeled in this manner to allow comparison of the actual velocity change of a drop with its corresponding velocity change produced by the shock pulse.

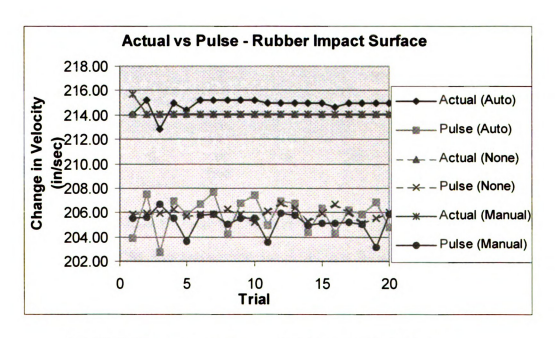


FIGURE 22: Δ_{actual} vs Δ_{pulse} - Rubber Impact Surface

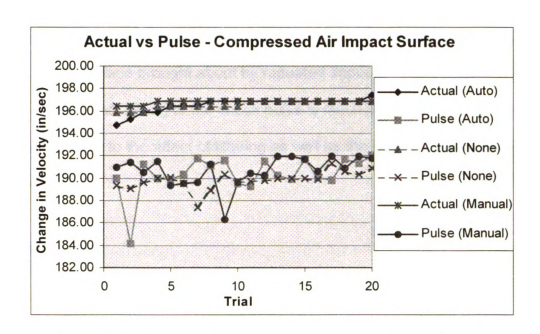


FIGURE 23: Δ_{actual} vs Δ_{pulse} – Compressed Air Impact Surface

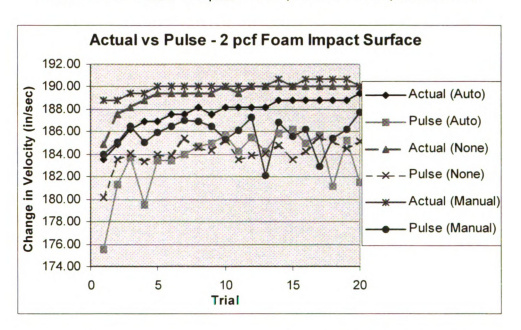


FIGURE 24: Δ_{actual} vs $\Delta_{\text{pulse}} - 2$ pcf Foam Cushion Impact Surface In Figures 22, 23, and 24, the actual change in velocity is consistently greater in magnitude than the change in velocity given by the shock pulse. This holds true for all the impact surfaces and methods of filtering. The variance in the actual velocity change was small because the experimental drops were identical (all

from 90°). Variance in the actual velocity change can be explained by adaptation of the impact surface brought about by repeated impacts. The variance in the velocity change according to the shock pulse is much greater than the actual and can be attributed to the affect of filtering as well as the inherent errors in the method.

3.3.4 REMOUNTING RESULTS

In order for the motion of the device to be accurately transmitted to the accelerometer, the accelerometer must be mounted properly. After initial testing, the accelerometer and adhesive were completely removed from the head of the hammer, the surface was cleaned, and the accelerometer was then remounted with a new adhesive. The remounting results are shown in Figures 25-27 for each impact surface and each method of filtering.

The accelerometer was remounted and re-examined to determine the sensitivity of the method to mounting errors. The effect of mounting errors can be quantified by comparing the initial test results with the results subsequent to remounting the accelerometer. Successful results will also validate the initial testing results.

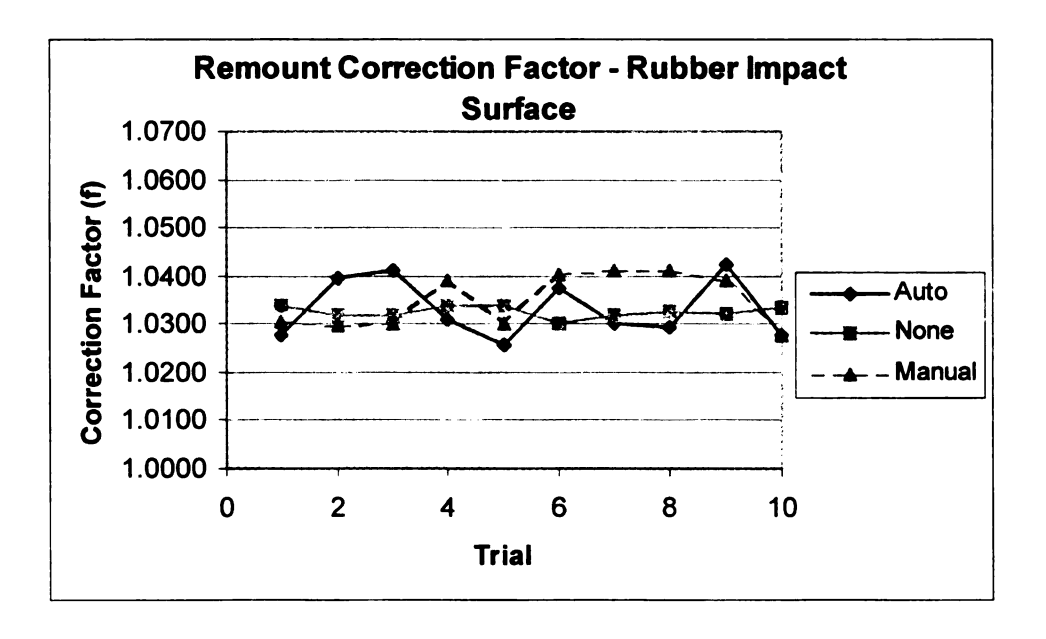


FIGURE 25: Correction Factor After Remount – Rubber Impact Surface

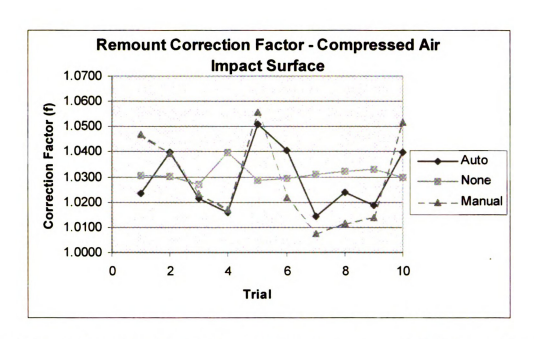


FIGURE 26: Correction Factor After Remount - Compressed Air Impact Surface

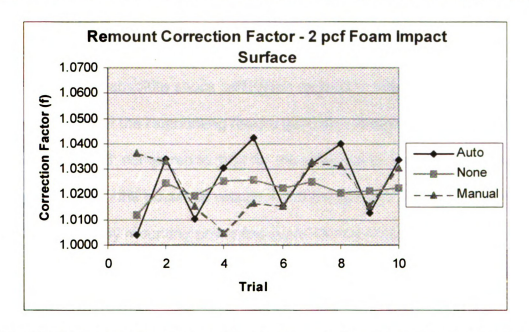


FIGURE 27: Correction Factor After Remount – 2 pcf Foam Impact Surface
The results produced by the impact surfaces after remounting the accelerometer
are similar to the initial results in the consistency of each filtering method, where
the method without filter was the most consistent. The correction factor
magnitudes, for each filtering method, are all also similar to the initial results.

The rubber impact surface remounting results, although, did reduce the average percent difference between the Δ_{actual} vs Δ_{pulse} , for the automatic filter, by 0.97%. The average percent difference was also reduced, for the unfiltered and manual filtering methods, by 0.65% and 0.76%, respectively. The other impact surfaces and filtering methods, while having some points in which the percent difference was reduced, were similar in magnitude and average.

Remounting and retesting the accelerometer provided validity to the initial results by recreating similar results. The percent difference between the Δ_{actual} vs Δ_{pulse} after remounting the accelerometer was similar to the initial testing, as low percentages of error in measurement were maintained for all impact surfaces and filtering methods. The minimal amounts of error in the results also prove the insensitivity of the absolute shock calibration method to mounting errors.

The fact that the remounting results gave an average correction factor of approximately 1.03, compared to 1.04 for the initial results, says that much of the difference between the observed results and the assumed "correct" value of 1.0 can be explained by mounting errors that have nothing to do with the method. A correction factor of 1.04 vs. 1.00 does not necessarily mean that the method has an inherent error of 0.4%. Add to this the fact that the manufacturer's or calibration laboratories uncertainty in the sensitivity is \pm 3%, means that there could actually be no error whatsoever in the method. (4)

CHAPTER 4

CONCLUSIONS

4.1 Method Accuracy

Methods of accelerometer calibration while being subjected to shock are generally unavailable. The principle usage of the absolute shock calibration method presented here is to calibrate piezoelectric accelerometers designed for use in shock measurements. The method has successfully evaluated the performance of a piezoelectric accelerometer by calculating the sensitivity of the accelerometer within 5.0% of its rated value. The method was evaluated for shock pulses, filtered and un-filtered, up to 70 g's of acceleration and as low as 25 g's of acceleration. Shock pulses of 30 g's or less produced a sensitivity that was within 4.0% of the rated value, and shock pulses at 30 g's or less, formed by impact onto a 2 pcf foam cushion, gave a sensitivity within 2.75%. The low percent differences prove the insensitivity of the calibration method to experimental and inherent errors.

The experimental errors were related to mounting the accelerometer, determining the natural frequency, and measuring the rebound angle after impact. The percent difference, although low, can most likely be attributed to these errors, and is proven further by the fact that remounting the accelerometer accounted for 1% of the initial 4% of error. This amount of error can be expected and is tolerated in the industry.

The inherent errors consisted of the transverse sensitivity and the actual sensitivity of the accelerometer. The transverse sensitivity of the accelerometer

does not become a major factor as long as the centripetal acceleration is held to a minimum. Centripetal acceleration is the force acting on the accelerometer that is not along its sensing axis. For the shock calibration method the centripetal acceleration acting on the accelerometer is approximately equal to 2 g's. However, the transverse sensitivity of the accelerometer will further reduce the effect of centripetal acceleration by 5%, thus quantifying the effect of centripetal acceleration on the shock pulse to be 0.1 g's.

Accelerometer calibration is expensive and time consuming, and, yet, uncertainties on the order of 3% can still be expected from manufacturers and calibration laboratories.

The principle advantages of the absolute shock calibration method over other methods of calibration are its ease of use, cost of implementation, and its actual use simulation of an accelerometer in the packaging laboratory.

4.2 Recommendations for Use

The correction factor for the sensitivity of an accelerometer could theoretically be determined by the difference between a current shock pulse and an initially established baseline shock pulse, provided the method and materials are the same for both shock pulses. The absolute shock calibration method is a repeatable method that has the ability to self-test the performance of the machine. Establishing an initial baseline shock pulse for a newly calibrated accelerometer and test materials will ensure accuracy in the results and procedure through comparison.

As expected, the no-filter method of signal filtering provided the most consistent results, and, because of this, the no-filter method should be used in the calibration of a piezoelectric accelerometer. Although the tolerance range was greater for the no-filter method, the absence of a filter significantly reduced the amount of variance in the change in velocity values provided by the shock pulse.

The impact surface of the absolute shock calibration method can be customized to simulate specific g-levels, and the results showed that piezoelectric accelerometer calibrations executed on a foam cushion performed well. Using foam cushions of varying densities can control the g-level, and such cushions are commonly used and tested in packaging laboratories. Using a foam impact surface for calibration will simulate the actual use of many accelerometers as well as provide excellent results in calibration.

The performance of the absolute shock calibration method for impact surfaces that create accelerations greater than 70 g's should be evaluated prior to implementation at elevated levels of acceleration. The tolerance range for the sensitivity calculation of piezoelectric accelerometers grew with the g-level, and further testing should be done to determine the true effect of higher levels of acceleration. The performance of an accelerometers' sensitivity is not known over a wide range of g's. The non-linear material properties of the piezoelectric material could cause the sensitivity of the accelerometer to change at higher g-levels. An example of this possibility is the fact that stress is proportional to strain for low levels of strain, but not for high levels of strain.

4.3 Design Recommendations

The absence of friction in the bearings is the single most important aspect of this absolute shock calibration method. The theory behind the method of calibration is based on the assumption of minimal friction in the bearings, despite the insensitivity of the device to friction. Energy lost to friction will decrease the speed of the hammer, and, in turn, will decrease the natural frequency of the hammer in pendulum motion as well as the magnitude of the rebound angle (θ_r) . However, the effect friction has on the correction factor may be minimal. The decrease in speed should decrease the ΔV_{actual} and the ΔV_{pulse} at similar magnitudes, thus having little effect on the correction factor.

The mounting technique of the accelerometer is an important aspect in the performance of the calibration method. The mounting surface and mounting technique of the calibration device should be manufactured with a permanent mounting technique to ensure repeatability.

APPENDICES

APPENDIX A MANUAL FILTER FREQUENCY DETERMINATION

The manual filter frequency recommended by many in industry is five times the shock pulse frequency. The shock pulse frequency is determined by viewing the shock pulse as half of a sine wave. So the shock pulse frequency is 1/(2 x pulse duration). The pulse duration is not easy to determine because the beginning and ends of the pulse are unclear due to noise. In Tables A1-A3 below, the pulse duration was determined over several trials for the filtered and auto filtered pulses.

	Shock Pulse	Duration (ms)	
į	None	Auto	
[13.30	14.00	
	13.40	13.70	
	13.35	13.95	
	13.30	13.60	
	13.35	13.90	
Ø	13.25	13.35	
Ball	13.30	13.45	
	13.30	13.35	
面	13.25	13.50	
ا ق	13.30	13.50	
<u></u>	13.25	13.45	
Rubber	13.30	13.50	
~	13.20	13.50	
	13.30	13.45	
1	13.25	13.50	
1	13.35	13.45	
1	13.25	13.45	
<u> </u>	13.30	13.45	
1	13.20	13.50	
	13.30	13.40	
VERAGE	13.29	13.55	13.42
	Filter Fr	equency (cps) =	186.31

TABLE A-1: Manual Filter Frequency for Rubber Impact Surface

67

Ĺ	Shock Pulse	Duration (ms)	
	None	Auto	
	28.25	30.50	
	28.45	29.90	
	28.50	30.60	
Ĺ	28.50	30.50	
=	28.55	30.50	
Ball	28.50	30.60	
m	28.70	30.75	
	28.60	30.65	
<u>်လ</u> [28.55	30.75	
Tennis	28.75	30.45	
	28.70	30.50	
<u>a</u>	28.55	30.80	
	28.75	30.65	
	28.80	30.60	
	28.60	30.80	
	28.60	30.60	
L	28.85	30.55	
	28.70	30.85	
	28.50	30.75	
	28.80	30.85	
AVERAGE	28.61	30.61	29.61
	Filter Fr	requency (cps) =	84.43

TABLE A-2: Manual Filter Frequency for Compressed Air Impact Surface

68

	Shock Pulse	Duration (ms)	
	None	Auto	
	24.65	24.75	
	24.40	24.95	
	24.40	25.10	
	24.15	24.85	
Ĺ	24.05	25.10	
	24.45	25.05	
	24.40	25.10	
	24.40	25.15	
Foam	24.40	25.20	
	24.25	25.25	
	24.30	25.05	
	24.15	25.30	
L	24.45	25.00	
	24.50	25.25	
	24.05	25.20	
	24.40	25.10	
	24.40	25.20	
	24.60	24.80	
ļ	24.40	25.05	
	24.40	24.75	-
VERAGE	24.36	25.06	24.71
	Filter Fr	equency (cps) =	101.1

TABLE A-3: Manual Filter Frequency for 2 pcf Foam Cushion Impact Surface

APPENDIX B INITIAL CALIBRATION RESULTS

Table B1-B9 show the experimental results for the actual velocity change and the velocity change from the shock pulse. The actual velocity change was calculated using Equation 26 in which the rebound angle is a variable. The rebound angles are shown in Tables B1-B9, while the other variables associated with Equation 26 are; b = 15.125", f_n = 0.8341 cps (from Table 1), and θ_d = 90°.

Trial	Rebound Angle (Degrees)	Change in Velocity - Actual (in/sec)	Change in Velocity - Pulse (in/sec)	Correction Factor (f)
1	56	214.07	203.92	1.0498
2	58	215.23	207.51	1.0372
3	54	212.83	202.77	1.0496
4	57.5	214.95	206.94	1.0387
5	56.5	214.37	205.87	1.0413
6	58	215.23	206.66	1.0415
7	58	215.23	207.66	1.0365
8	58	215.23	204.25	1.0538
9	58	215.23	206.78	1.0409
10	58	215.23	207.38	1.0379
11	57.5	214.95	204.93	1.0489
12	57.5	214.95	206.90	1.0389
13	57.5	214.95	206.73	1.0398
14	57.5	214.95	204.37	1.0518
15	57.5	214.95	206.37	1.0416
16	57	214.66	204.33	1.0506
17	57.5	214.95	206.20	1.0424
18	57.5	214.95	205.87	1.0441
19	57.5	214.95	206.82	1.0393
20	57.5	214.95	204.80	1.0496
AVERAGE	57.3	214.84	205.85	1.0437
Std. Dev.	0.9358	0.5588	1.3863	0.0055

TABLE B-1: Results – Rubber Impact Surface and Auto Filter

Trial	Rebound Angle (Degrees)	Change in Velocity - Actual (in/sec)	Change in Velocity - Pulse (in/sec)	Correction Factor (f)
1	56	214.07	205.87	1.0398
2	56	214.07	205.94	1.0395
3	56	214.07	205.95	1.0394
4	56	214.07	206.29	1.0377
5	56	214.07	205.66	1.0409
6	56	214.07	205.84	1.0400
7	56	214.07	205.84	1.0400
8	56	214.07	206.30	1.0377
9	56	214.07	205.88	1.0398
10	56	214.07	205.21	1.0432
11	56	214.07	206.11	1.0386
12	56	214.07	206.72	1.0356
13	56	214.07	206.31	1.0376
14	56	214.07	205.25	1.0430
15	56	214.07	205.97	1.0393
16	56	214.07	206.71	1.0356
17	56	214.07	206.04	1.0390
18	56	214.07	205.15	1.0435
19	56	214.07	205.56	1.0414
20	56	214.07	205.99	1.0392
AVERAGE	56.00	214.07	205.93	1.0395
Std. Dev.	0.0000	0.0000	0.4301	0.0022

TABLE B-2: Results – Rubber Impact Surface and No Filter

Trial	Rebound Angle (Degrees)	Change in Velocity - Actual (in/sec)	Change in Velocity – Pulse (in/sec)	Correction Factor (f)
1	58.8	215.68	205.55	1.0493
2	56	214.07	205.63	1.0410
3	56	214.07	206.67	1.0358
4	56	214.07	205.53	1.0416
5	56	214.07	203.61	1.0514
6	56	214.07	205.77	1.0403
7	56	214.07	205.82	1.0401
8	56	214.07	205.03	1.0441
9	56	214.07	205.56	1.0414
10	56	214.07	205.52	1.0416
11	56	214.07	203.60	1.0514
12	56	214.07	205.94	1.0395
13	56	214.07	205.79	1.0402
14	56	214.07	204.99	1.0443
15	56	214.07	205.15	1.0435
16	56	214.07	205.08	1.0438
17	56	214.07	205.22	1.0431
18	56	214.07	205.05	1.0440
19	56	214.07	203.11	1.0540
20	56	214.07	205.82	1.0401
AVERAGE	56.14	214.15	205.22	1.0435
Std. Dev.	0.6261	0.3594	0.8693	0.0046

TABLE B-3: Results – Rubber Impact Surface and Manual Filter

Trial	Rebound Angle (Degrees)	Change in Velocity - Actual (in/sec)	Change in Velocity - Pulse (in/sec)	Correction Factor (f)
1	33	194.74	189.93	1.0253
2	33.5	195.29	184.13	1.0606
3	34	195.84	191.21	1.0242
4	34	195.84	189.95	1.0310
5	34.5	196.38	189.87	1.0343
6	34.5	196.38	190.37	1.0315
7	34.5	196.38	191.72	1.0243
8	35	196.91	191.17	1.0300
9	35	196.91	191.59	1.0278
10	35	196.91	189.52	1.0390
11	35	196.91	189.28	1.0403
12	35	196.91	191.49	1.0283
13	35	196.91	190.27	1.0349
14	35	196.91	189.90	1.0369
15	35	196.91	191.63	1.0275
16	35	196.91	190.04	1.0361
17	35	196.91	189.76	1.0377
18	35	196.91	191.66	1.0274
19	35	196.91	191.35	1.0290
20	35.5	197.43	192.07	1.0279
AVERAGE	34.68	196.56	190.35	1.0327
STD. DEV.	0.6129	0.6603	1.7042	0.0082

TABLE B-4: Results – Compressed Air Impact Surface and Auto Filter

Trial	Rebound Angle (Degrees)	Change in Velocity - Actual (in/sec)	Change in Velocity - Pulse (in/sec)	Correction Factor (f)
1	34	195.84	189.31	1.0345
2	34	195.84	189.09	1.0357
3	34	195.84	189.58	1.0330
4	34.5	196.38	189.97	1.0337
5	34.5	196.38	190.04	1.0333
6	34.5	196.38	189.53	1.0361
7	34.5	196.38	187.40	1.0479
8	34.5	196.38	188.91	1.0395
9	34.5	196.38	190.30	1.0319
10	34.5	196.38	189.67	1.0354
11	35	196.91	189.68	1.0381
12	35	196.91	189.82	1.0373
13	35	196.91	189.97	1.0365
14	35	196.91	189.95	1.0366
15	35	196.91	189.97	1.0365
16	35	196.91	189.84	1.0372
17	35	196.91	191.28	1.0294
18	35	196.91	190.62	1.0330
19	35	196.91	190.29	1.0348
20	35	196.91	190.88	1.0316
AVERAGE	34.675	196.5611487	189.805	1.035608515
STD. DEV.	0.3726	0.3984	0.7992	0.0038

TABLE B-5: Results – Compressed Air Impact Surface and No Filter

Trial	Rebound Angle (Degrees)	Change in Velocity - Actual (in/sec)	Change in Velocity - Pulse (in/sec)	Correction Factor (f)
1	34.5	196.38	190.94	1.0285
2	34.5	196.38	191.41	1.0259
3	34.5	196.38	190.54	1.0306
4	35	196.91	191.52	1.0281
5	35	196.91	189.36	1.0399
6	35	196.91	189.54	1.0389
7	35	196.91	189.60	1.0385
8	35	196.91	191.21	1.0298
9	35	196.91	186.34	1.0567
10	35	196.91	189.62	1.0384
11	35	196.91	190.45	1.0339
12	35	196.91	190.28	1.0348
13	35	196.91	191.94	1.0259
14	35	196.91	191.94	1.0259
15	35	196.91	191.71	1.0271
16	35	196.91	190.57	1.0333
17	35	196.91	191.92	1.0260
18	35	196.91	190.83	1.0319
19	35	196.91	191.93	1.0259
20	35	196.91	191.72	1.0271
AVERAGE	34.93	196.83	190.67	1.0324
STD. DEV.	0.1832	0.1949	1.3463	0.0075

TABLE B-6: Results – Compressed Air Impact Surface and Manual Filter

Trial	Rebound Angle (Degrees)	Change in Velocity - Actual (in/sec)	Change in Velocity – Pulse (in/sec)	Correction Factor (f)
1	24	183.51	175.52	1.0455
2	25	184.89	181.35	1.0195
3	26	186.24	183.75	1.0135
4	26.5	186.89	179.54	1.0410
5	26.5	186.89	183.48	1.0186
6	27	187.55	183.42	1.0225
7	27	187.55	184.00	1.0193
8	27.5	188.19	184.73	1.0187
9	27	187.55	184.98	1.0139
10	27.5	188.19	185.64	1.0137
11	27.5	188.19	184.24	1.0214
12	27.5	188.19	185.53	1.0143
13	27.5	188.19	184.26	1.0213
14	28	188.82	185.87	1.0159
15	28	188.82	186.23	1.0139
16	28	188.82	184.94	1.0210
17	28	188.82	185.68	1.0169
18	28	188.82	181.15	1.0423
19	28	188.82	185.22	1.0194
20	28.5	189.45	181.45	1.0441
AVERAGE	27.15	187.72	183.55	1.0228
STD. DEV.	1.1133	1.4648	2.6194	0.0109

TABLE B-7: Results – 2 pcf Foam Impact Surface and Auto Filter

Trial	Rebound Angle (Degrees)	Change in Velocity - Actual (in/sec)	Change in Velocity – Pulse (in/sec)	Correction Factor (f)
1	25	184.89	180.16	1.0263
2	27	187.55	183.53	1.0219
3	27.5	188.19	184.04	1.0225
4	28	188.82	183.39	1.0296
5	28.5	189.45	184.00	1.0296
6	28.5	189.45	183.93	1.0300
7	28.5	189.45	185.38	1.0219
8	28.5	189.45	184.57	1.0264
9	28.5	189.45	184.36	1.0276
10	29	190.07	185.24	1.0261
11	28.5	189.45	183.55	1.0321
12	29	190.07	183.87	1.0337
13	29	190.07	184.11	1.0323
14	29	190.07	184.74	1.0288
15	29	190.07	183.53	1.0356
16	29	190.07	184.26	1.0315
17	29	190.07	185.47	1.0248
18	29	190.07	185.18	1.0264
19	29	190.07	184.51	1.0301
20	29	190.07	185.10	1.0268
AVERAGE	28.43	189.34	184.15	1.0282
STD. DEV.	0.9770	1.2557	1.1449	0.0038

TABLE B-8: Results – 2 pcf Foam Impact Surface and No Filter

Trial	Rebound Angle (Degrees)	Change in Velocity - Actual (in/sec)	Change in Velocity – Pulse (in/sec)	Correction Factor (f)
1	28	188.82	183.95	1.0265
2	28	188.82	185.04	1.0204
3	28.5	189.45	186.48	1.0159
4	28.5	189.45	185.07	1.0237
5	29	190.07	185.92	1.0223
6	29	190.07	186.44	1.0194
7	29	190.07	187.01	1.0163
8	29	190.07	186.88	1.0170
9	29	190.07	186.48	1.0192
10	29	190.07	185.35	1.0254
11	29	190.07	186.16	1.0210
12	29	190.07	187.32	1.0147
13	29	190.07	182.15	1.0435
14	29.5	190.68	186.79	1.0208
15	29	190.07	185.59	1.0241
16	29.5	190.68	186.25	1.0238
17	29.5	190.68	182.91	1.0425
18	29.5	190.68	185.44	1.0282
19	29.5	190.68	186.21	1.0240
20	29	190.07	187.75	1.0123
AVERAGE	28.98	190.03	185.76	1.0231
STD. DEV.	0.4435	0.5477	1.4165	0.0080

TABLE B-9: Results – 2 pcf Foam Impact Surface and Manual Filter

APPENDIX C REMOUNT CALIBRATION RESULTS

Appendix C is the same as Appendix B except that the trials were conducted after remounting the accelerometer. The results are shown in Tables C1-C9.

Trial	Rebound Angle (Degrees)	Change in Velocity - Actual (in/sec)	Change in Velocity – Pulse (in/sec)	Correction Factor (f)
1	56	214.07	207.75	1.0304
2	56	214.07	207.91	1.0296
3	56	214.07	207.83	1.0300
4	56	214.07	206.00	1.0392
5	56	214.07	207.79	1.0302
6	56	214.07	205.76	1.0404
7	56	214.07	205.58	1.0413
8	56	214.07	205.63	1.0410
9	56	214.07	205.99	1.0392
10	56	214.07	208.31	1.0277
AVERAGE	56.00	214.07	206.86	1.0349
STD. DEV.	0.0000	0.0000	1.1382	0.0057

TABLE C-3: Remount Results – Rubber Impact Surface and Manual Filter

Trial	Rebound Angle (Degrees)	Change in Velocity - Actual (in/sec)	Change in Velocity – Pulse (in/sec)	Correction Factor (f)
1	35	196.91	192.42	1.0233
2	34.5	196.38	188.89	1.0396
3	35	196.91	192.77	1.0215
4	35.5	197.43	194.31	1.0161
5	35.5	197.43	187.88	1.0508
6	36	197.95	190.22	1.0407
7	36	197.95	195.18	1.0142
8	36	197.95	193.31	1.0240
9	36	197.95	194.34	1.0186
10	36	197.95	190.37	1.0398
AVERAGE	35.55	197.48	191.97	1.0289
STD. DEV.	0.5503	0.5768	2.4916	0.0127

TABLE C-4: Remount Results – Compressed Air Impact Surface and Auto Filter

Trial	Rebound Angle (Degrees)	Change in Velocity - Actual (in/sec)	Change in Velocity – Pulse (in/sec)	Correction Factor (f)
1	36	197.95	192.08	1.0306
2	36	197.95	192.13	1.0303
3	36	197.95	192.73	1.0271
4	36	197.95	190.39	1.0397
5	36	197.95	192.45	1.0286
6	36	197.95	192.26	1.0296
7	36	197.95	191.99	1.0311
8	36	197.95	191.80	1.0321
9	36	197.95	191.64	1.0329
10	36	197.95	192.20	1.0299
AVERAGE	36.00	197.95	191.97	1.0312
STD. DEV.	0.0000	0.0000	0.6340	0.0034

TABLE C-5: Remount Results – Compressed Air Impact Surface and No Filter

Trial	Rebound Angle (Degrees)	Change in Velocity - Actual (in/sec)	Change in Velocity – Pulse (in/sec)	Correction Factor (f)
1	36	197.95	189.08	1.0469
2	36	197.95	190.47	1.0393
3	36.5	198.47	193.91	1.0235
4	36	197.95	194.62	1.0171
5	36.5	198.47	187.99	1.0557
6	36.5	198.47	194.20	1.0220
7	36	197.95	196.48	1.0075
8	36	197.95	195.67	1.0117
9	36.5	198.47	195.74	1.0139
10	36	197.95	188.19	1.0519
AVERAGE	36.20	198.16	192.64	1.0289
STD. DEV.	0.2582	0.2648	3.3385	0.0179

TABLE C-6: Remount Results – Compressed Air Impact Surface and Manual Filter

Trial	Rebound Angle (Degrees)	Change in Velocity - Actual (in/sec)	Change in Velocity – Pulse (in/sec)	Correction Factor (f)
1	26	186.24	185.47	1.0041
2	27	187.55	181.37	1.0340
3	27.5	188.19	186.30	1.0101
4	27.5	188.19	182.60	1.0306
5	28	188.82	181.19	1.0421
6	28	188.82	185.94	1.0155
7	28	188.82	182.95	1.0321
8	28.5	189.45	182.20	1.0398
9	28.5	189.45	187.07	1.0127
10	28.5	189.45	183.26	1.0338
AVERAGE	27.75	188.50	183.84	1.0255
STD. DEV.	0.7906	1.0133	2.1610	0.0135

TABLE C-7: Remount Results – 2 pcf Foam Impact Surface and Auto Filter

Trial	Rebound Angle (Degrees)	Change in Velocity - Actual (in/sec)	Change in Velocity – Pulse (in/sec)	Correction Factor (f)
1	28.5	189.45	187.19	1.0121
2	28.5	189.45	184.93	1.0244
3	29	190.07	186.44	1.0194
4	29	190.07	185.38	1.0253
5	29	190.07	185.33	1.0256
6	29	190.07	185.90	1.0224
7	29	190.07	185.42	1.0251
8	29	190.07	186.25	1.0205
9	29.5	190.68	186.71	1.0212
10	29	190.07	185.89	1.0225
AVERAGE	28.95	190.00	185.94	1.0218
STD. DEV.	0.2838	0.3492	0.7057	0.0040

TABLE C-8: Remount Results – 2 pcf Foam Impact Surface and No Filter

Trial	Rebound Angle (Degrees)	Change in Velocity - Actual (in/sec)	Change in Velocity – Pulse (in/sec)	Correction Factor (f)
1	29	190.07	183.38	1.0365
2	29.5	190.68	184.56	1.0331
3	29.5	190.68	187.79	1.0154
4	29.5	190.68	189.75	1.0049
5	29.5	190.68	187.58	1.0165
6	29.5	190.68	187.79	1.0154
7	29.5	190.68	184.59	1.0330
8	29.5	190.68	184.93	1.0311
9	29.5	190.68	187.80	1.0153
10	29.5	190.68	185.06	1.0303
AVERAGE	29.45	190.61	186.32	1.0231
STD. DEV.	0.1581	0.1930	2.0580	0.0108

TABLE C-9: Remount Results – 2 pcf Foam Impact Surface and Manual Filter

BIBLIOGRAPHY

- 1. Accelerometers and How They Work, Texas Instruments. 2005. Retrieved from http://www2.usfirst.org/2005comp/manual/acceler1.pdf
- 2. Structural Gravimetric Calibration System, The Modal Shop, Inc. 2006. Retrieved from http://www.modalshop.com/test_calibration.asp?ID=85
- Mechanical Measurements Calibration Services, The National Institute of Standars and Technology. 2006. http://ts.nist.gov/ts/htdocs/230/233/calibrations/mechanical/vibration.htm
- 4. Why Calibrate a Transducer?, The Modal Shop, Inc. 2006. Retrieved from http://www.modalshop.com/%5Ctest_calibration.asp?ID=83
- 5. Bouche, R.R., *The Absolute Calibration of Pickups on a Drop-Ball Shock Machine of the Ballistic Type*. 1961, Endevco Corporation. Retrieved from http://www.endevco.com/resources/techpapers.php
- 6. Bouche, D.R.R., *Accurate Accelerometer Calibrations by Absolute and Comparison Methods*. 1966, Endevco Corporation. Retrieved from http://www.endevco.com/resources/techpapers.php
- 7. Burgess, D.G., *Distribution Packaging Dynamics*. 2004: School of Packaging Michigan State University.
- 8. Burgess, D.G., *Advanced Distribution Packaging Dynamics*. 2005: School of Packaging Michigan State University.
- 9. Evans, B.P.a.D.J., Comparison of Results of Calibrating the Magnitude of the Sensitivity of Accelerometers by Laser Interferometry and Reciprocity. 1999, The National Institute of Standards and Technology.
- 10. Halliday, R.R.a.D., *Physics Part 1*. 1977, John Wiley & Sons.
- 11. Kipp, B., Signal Filtering Part 1. Lansmont, Inc. Retrieved from http://www.lansmont.com/newsletters/html/95-07-p3.htm
- 12. Kipp, B., Signal Filtering Part 2: Practical Application. Lansmont, Inc. Retrieved from http://www.lansmont.com/newsletters/html/95-07-p3.htm
- 13. Matthews, J., *Technical Paper 319 Guide to accelerometer Installation*, Endevco Corporation.

BIBLIOGRAPHY (con't)

- 14. Matthews, J., Technical Paper 312 Guide to Adhesively Mounting Accelerometers, Endevco Corporation.
- 15. Piezoelectric Accelerometers for Vibration and Shock Measurements.
 Oceana Sensor Technologies, Inc.
- 16. Ramage, I., *Understanding Transverse Sensitivity*, Sensorland.com. Retrieved from http://www.sensorland.com/howpage052.htm
- 17. Rust, K.J., Introduction to Accelerometers and Calibration Techniques. 1997, MTS Systems Corporation.
- 18. Schnellinger, G.K.a.J., *The Principles of Piezoelectric Accelerometers*, in *Sensors Magazine*. Retrieved from http://www.sensorsmag.com/sensors/article/articledetail.jsp?id=357608
- 19. Shkel, A.M.a.C.A., Experimental Evaluation and Comparative Analysis of Commercial Variable-Capacitance MEMS Accelerometers. The Journal of Micromechanics and Microengineering, 2003. Volume 13: p. 634-645.

GENERAL RESOURCES

- 1. *IEEE Standard Specification Format Guide and Test Procedure for Linear, Single-Axis, Nongyroscopic Accelerometers.* 1999: The Institute of Electrical and Electronics Engineers.
- 2. C.H. Edwards, J.a.D.E.P., *Calculus and Analytical Geometry*. Second Edition ed. 1986: Prentice-Hall, Inc.
- 3. DiPrima, W.E.B.a.R.C., *Introduction to Differential Equations*. 1970: John Wiley & Sons.
- 4. Marek Dobosz, T.U.a.T.K., *Methods for the Calibration of Vibration Pickups by Laser Interferometry: I. Theoretical Analysis.* 1997, National Research Laboratory of Metrology.
- 5. Mark Harrison, A.O.S., and Paul G. Marcotte, *The Reciprocity Calibration of Piezoelectric Accelerometers*. The Journal of the Acoustical Society of America, 1952. **Volume 24**(Number 4): p. 384-389.